EXPERIMENTAL CALIBRATION OF A VECTOR ELECTRIC FIELD
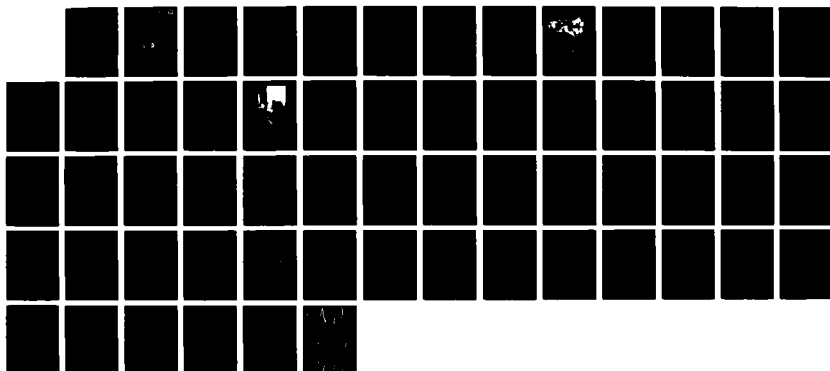METER MEASUREMENT SYSTEM ON AN AIRCRAFT(U) NAVAL
RESEARCH LAB WASHINGTON DC J C BAILEY ET AL. 13 MAR 87

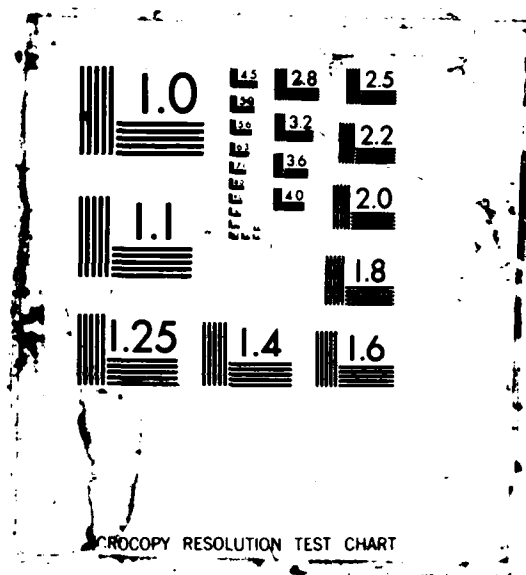UNCLASSIFIED   NRL-MR-5900   F/G 1/3   NL
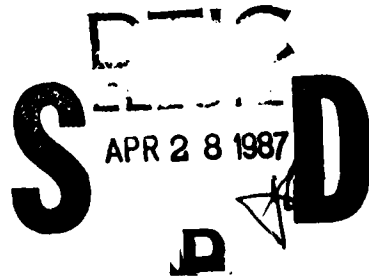
MICROCOPY RESOLUTION TEST CHART

Experimental Calibration of a Vector Electric Field Meter Measurement System on an Aircraft

J. C. BAILEY AND R. V. ANDERSON

Atmospheric Physics Branch
Space Science Division

March 13, 1987

APR 2 8 1987

REPORT DOCUMENTATION PAGE

1a REPORT SECURITY CLASSIFICATION	1b RESTRICTIVE MARKINGS
UNCLASSIFIED	AD-A179357

2a. SECURITY CLASSIFICATION AUTHORITY	3 DISTRIBUTION / AVAILABILITY OF REPORT
2b DECLASSIFICATION / DOWNGRADING SCHEDULE	Approved for public release; distribution unlimited.

4 PERFORMING ORGANIZATION REPORT NUMBER(S)	5 MONITORING ORGANIZATION REPORT NUMBER(S)
NRL Memorandum Report 5900	

6a NAME OF PERFORMING ORGANIZATION	6b OFFICE SYMBOL (If applicable)	7a NAME OF MONITORING ORGANIZATION
Naval Research Laboratory	Code 4110	

6c. ADDRESS (City, State, and ZIP Code)	7b ADDRESS (City, State, and ZIP Code)
Washington, DC 20375-5000	

8a NAME OF FUNDING / SPONSORING ORGANIZATION	8b OFFICE SYMBOL (If applicable)	9 PROCUREMENT INSTRUMENT IDENTIFICATION NUMBER
Office of Naval Research		

8c. ADDRESS (City, State, and ZIP Code)	10 SOURCE OF FUNDING NUMBERS			
	PROGRAM ELEMENT NO.	PROJECT NO	TASK NO	WORK UNIT ACCESSION NO
Arlington, VA 22217	61153N	RR033-03-042		DN155-016

11 TITLE (Include Security Classification)

Experimental Calibration of a Vector Electric Field Meter Measurement System on an Aircraft

12 PERSONAL AUTHOR(S)
Bailey, J. C. and Anderson, R. V.

13a TYPE OF REPORT	13b TIME COVERED	14 DATE OF REPORT (Year, Month, Day)	15 PAGE COUNT
Interim	FROM _____ TO _____	1987 March 13	61

16 SUPPLEMENTARY NOTATION

17	COSATI CODES		18 SUBJECT TERMS (Continue on reverse if necessary and identify by block number)
FIELD	GROUP	SUB-GROUP	Electrostatic field Calibration
			Aircraft Field mills

19 ABSTRACT (Continue on reverse if necessary and identify by block number)

Although numerous aircraft have been instrumented with field mills, there have been few instances of reports of the absolute calibration of any of the three field components or self charge. Furthermore, a full vector calibration of all components has never been satisfactorily reported. This report outlines the various resons why a full vector calibration is difficult to obtain and suggests ways of avoiding the pitfalls. A full vector calibration is presented for a CV-580 turboprop aircraft. Errors are estimated for all components and various improvements are suggested.

20 DISTRIBUTION / AVAILABILITY OF ABSTRACT	21 ABSTRACT SECURITY CLASSIFICATION
☐ UNCLASSIFIED/UNLIMITED ☐ SAME AS RPT ☐ DTIC USERS	UNCLASSIFIED

22a NAME OF RESPONSIBLE INDIVIDUAL	22b TELEPHONE (Include Area Code)	22c OFFICE SYMBOL
J. C. Bailey	(202) 767-2977	Code 4110

OD FORM 1473, 84 MAR
83 APR edition may be used until exhausted
All other editions are obsolete

☆U.S. Government Printing Office: 1985—507-047

CONTENTS

iii

EXPERIMENTAL CALIBRATION OF A VECTOR ELECTRIC FIELD METER MEASUREMENT SYSTEM ON AN AIRCRAFT

I. INTRODUCTION

The measurement of the electrostatic field in the atmosphere can be made both at ground level and at altitude. Ground based measurements can only provide guesses as to the field conditions occurring within a cloud. They are not _in situ_ measurements. Altitude measurements can be made with both balloons and aircraft. Aircraft have several advantages over balloons. Statistical averages can be performed over an area; thus helping to filter effects such as local production of aerosols and space charges. Balloon measurements, such as performed by Mühleisen [1971] are more sensitive to these local variations. The aircraft, a more mobile and steerable platform, can more easily investigate many geographical conditions. The disadvantages of the aircraft are the higher self charge and exhaust space charges caused by the engines and the difficulty in obtaining the form factors needed for absolute calibration. The costs also tend to be higher. An aircraft based platform was chosen for our measurements.

Electrostatic fields have been measured aboard aircraft with shutter type field mills for several decades. Calibration includes the determination of the enhancement coefficients which relate the fields seen at a particular location on the aircraft skin to the true external fields. Some of the investigators are Gunn et. al. [1946], Clark [1958], Anderson [1966], Imianitov and Chubarina [1967], Fitzgerald and Byers [1958], Pelton et. al. [1953], Bly and Nanevicz [1977], Christian et. al. [1983], and Larouche et. al. [1985a]. Gunn et. al. [1946] and Imianitov and Chubarina [1967] did not install the required number of 4 mills necessary in order to resolve the field into its components. Clark [1958] and Anderson [1966] had four field mill installations, but only calibrated two of the three vector components. Fitzgerald and Byers [1962] indicate the capability of calculating all three

components of the vector electrostatic field and aircraft self charge, but further scrutiny indicates that several questionable symmetry assumptions have been made (e. g. - the belly mills located near the nose and the tail have the same sensitivity to a field directed along the nose-to-tail axis). Also, one coefficient was not calculated, the authors stating that "further flight measurements will be made." Furthermore, no estimate of the error of the measured fields is given. Larouche et. al. [1985b] and Bly and Nanevicz [1977] also indicate resolving of the field components; however, both calibrations are based on scale model measurements done in an applied external field. These measurements are suspect due to the inability to accurately model the exact field meter location and exposure. Pelton et. al. [1953] use sophisticated equipment in order to keep the self charge of the aircraft near zero. They make a reasonable calculation of the aircraft self charge, but a determination of the enhancement coefficients is apparently not performed. Jones et. al. [1985] indicates that a full vector calibration is near completion for the New Mexico Tech aircraft.

The statistically observed higher strike rate to aircraft in flight leads to the hypothesis that most lightning strikes to aircraft are triggered by the intrusion of the aircraft into a region of sufficient electrical energy density. During the summers of 1984 and 1985, a joint lightning strike project [USAF Flight Dynamics Lab (USAF/FDL), Federal Aviation Administration Atlantic City Technical Center (FAA/ACT), NASA Kennedy Space Flight Center (NASA/KSC), Office National d'Etudes et de Recherches Aerospatiales (ONERA), and Naval Research Lab (NRL)], was performed where an instrumented CV-580 turboprop aircraft was flown into thunderstorms. NRL's installation consisted of four shutter field mills. This would allow investigation of the triggering hypothesis if a full vector calibration is obtained. This report focuses on the problems associated with the calibration procedure. A similar less detailed report has been given by Anderson and Bailey [1986a]. This report supersedes the previous one.

Because of the considerable time and expense involved in installing field mills in an aircraft, design considerations along with the appropriate placement of the field meters on the aircraft must have prime consideration. After installation, the form factors must be obtained. The problems encountered during the calibration procedure will be addressed. A matrix of enhancement coefficients will be defined in terms of the field mill locations.

The determination of these enhancement coefficients with aircraft maneuvers in a fair weather field will be described. Error estimates are made for all the enhancement coefficients. Since the ultimate goal is studying the fields at the mill, the true external fields, and the self charge in relation to the triggering hypothesis; the enhancement matrix must be inverted. A Monte Carlo technique will be used to estimate the standard deviations associated with the inverted matrix, the external fields, and the self charge. Finally, some improvements that are suggested by the analysis will be enumerated.

II. FIELD MILL DESIGN

The calibration of field mills on an instrumented aircraft could be done both experimentally and theoretically. Estimation of errors are difficult in theoretical calculations; therefore, an experimental calibration was performed for the CV-580 aircraft. Experimental calibrations require a known, constant, and homogeneous field against which to calibrate. The vertical fair weather field can have these attributes along with the added advantage of only one component to measure; therefore, it was chosen as our calibration standard.

The proper choice of design characteristics of field mills can be critical to the calibration of an aircraft since fair weather fields can be as low as tens of volts per meter. Although aluminum is an attractive construction material from weight considerations it can have severe problems arising from contact potentials if used in the sensing areas. Laboratory tests performed at NRL [Willett and Bailey, 1983] indicate that non-magnetic 304 stainless steel gives good results with respect to reduced contact potentials. Earlier experiences indicate that spacings between the rotor and stator of several mm can further assist in reducing the effects of contact potentials without seriously reducing the sensitivity of the field mill. The desired measurement capabilities dictate the area of the sensor, the number of blades, and the rotational speed since these in turn determine the field meter's sensitivity and frequency response. A wide dynamic range is required if both fair and foul weather fields are to be measured. Exposure of the sensing area to undesired charges must be eliminated since they will be indistinguishable from true fields; therefore, insulators, which inevitably

build up surface charges, must be guarded from the moving parts of the sensing area. Rotor grounding is also of importance because synchronous currents flowing to the rotor through noisy or high resistance contact can produce error signals. For low level signals, a synchronous demodulator is necessary in order to recover the signal from the noise. The power, signal and reference paths must be diligently shielded to minimize extraneous signals. Finally, the power frequency should be filtered from the signal and reference paths.

The schematic field meter design and a picture of the final product are shown in fig 1. Dimensions of the CV-580 aircraft constrained the diameter to 3.25 inches (8.26 cm). A two bladed design with a rotation speed of 8000 rpm yielded a signal frequency of 266.7 Hz. Rotor grounding was provided by silver graphite brushes against a coin silver slip ring. Previous experience indicated that brass and carbide brushes are inferior with respect to rotational noise. [The group at New Mexico Tech immerses the back of the rotor shaft in a pool of mercury with good success (J. J. Jones, personal communication)]. A stainless steel shell surrounding the sensing parts during operation insures that contact potentials between the sensing parts and the aircraft body are kept at a minimum. The relative phase of the rotor with respect to the stator is generated at the back of the motor unit by a magnetic rotor and can be mechanically adjusted, by the phase adjusting ring, through 360 electrical degrees. The overall design of this field meter system facilitates cleaning of the rotor, stator, and insulators which is essential to operation in fair weather calibrations. Time and monetary constraints prohibited a dual-stator differential design that could have doubled the signal strength.

The signals from the field meter heads were transmitted along separate anti-microphonic cables (RG-149/U - essential in order to eliminate noise) to amplifiers inside the aircraft. In order to facilitate repairs and to conserve space at the field meter head, the preamplifier (fig. 2) was located at the amplifier end of the anti-microphonic cable. Since a field mill is a current generator, the preamplifier was configured as a current sensor. This maintains the stator voltage near ground which helps eliminate leakages due to voltage drops across the insulators. The preamplifier is completely shielded from the rest of the amplifier stages, is heavily decoupled at the
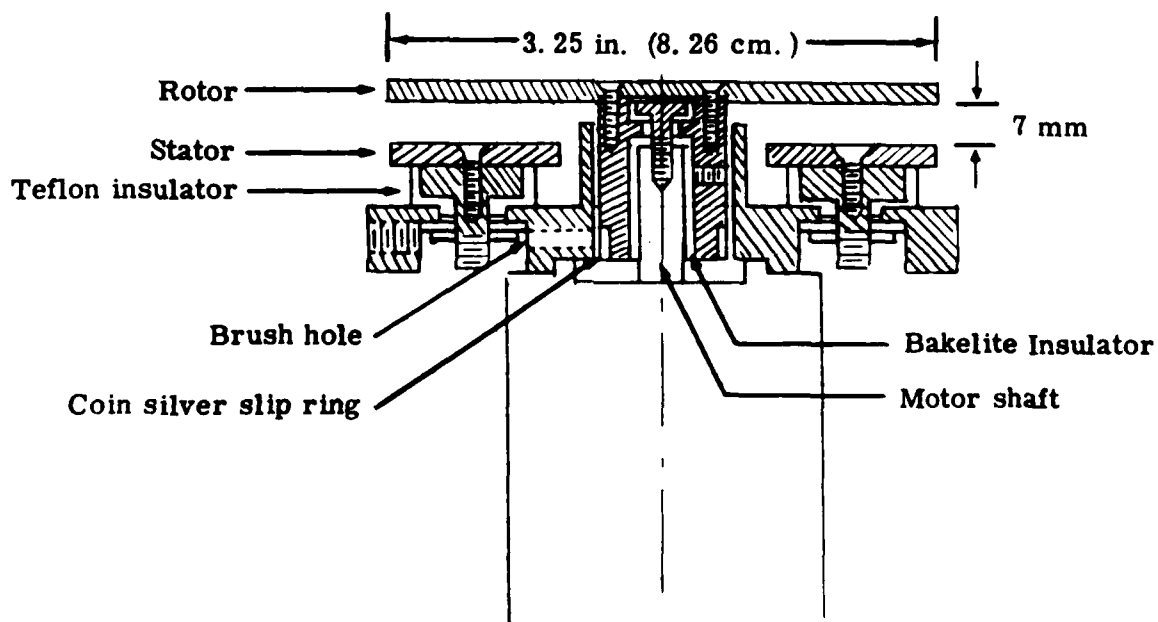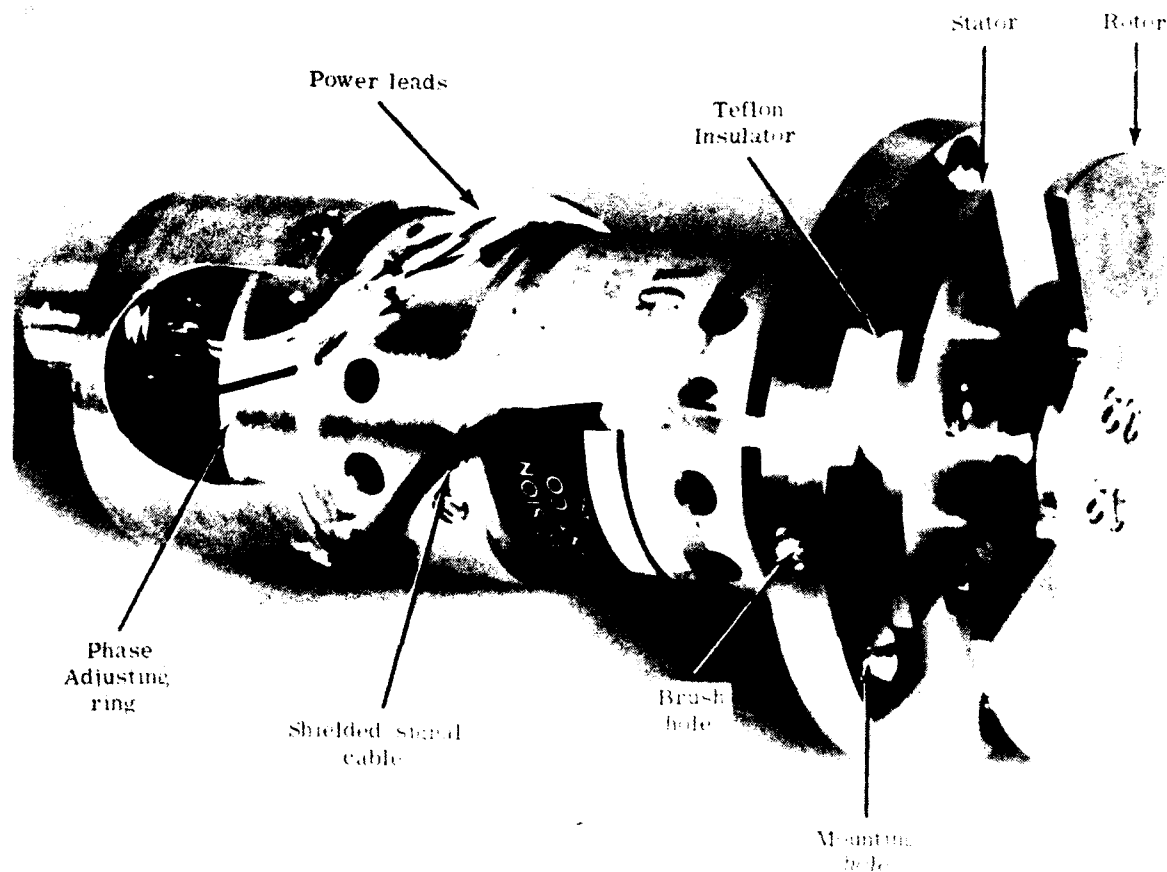
4

Power leads

Teflon
Insulator

Stator   Rotor

Phase
Adjusting
ring

Brush
hole

Shielded signal
cable

Mounting
hole

|←————— 3.25 in. (8.26 cm.) —————→|

Rotor

Stator

Teflon insulator

7 mm

Brush hole

Coin silver slip ring

Bakelite Insulator
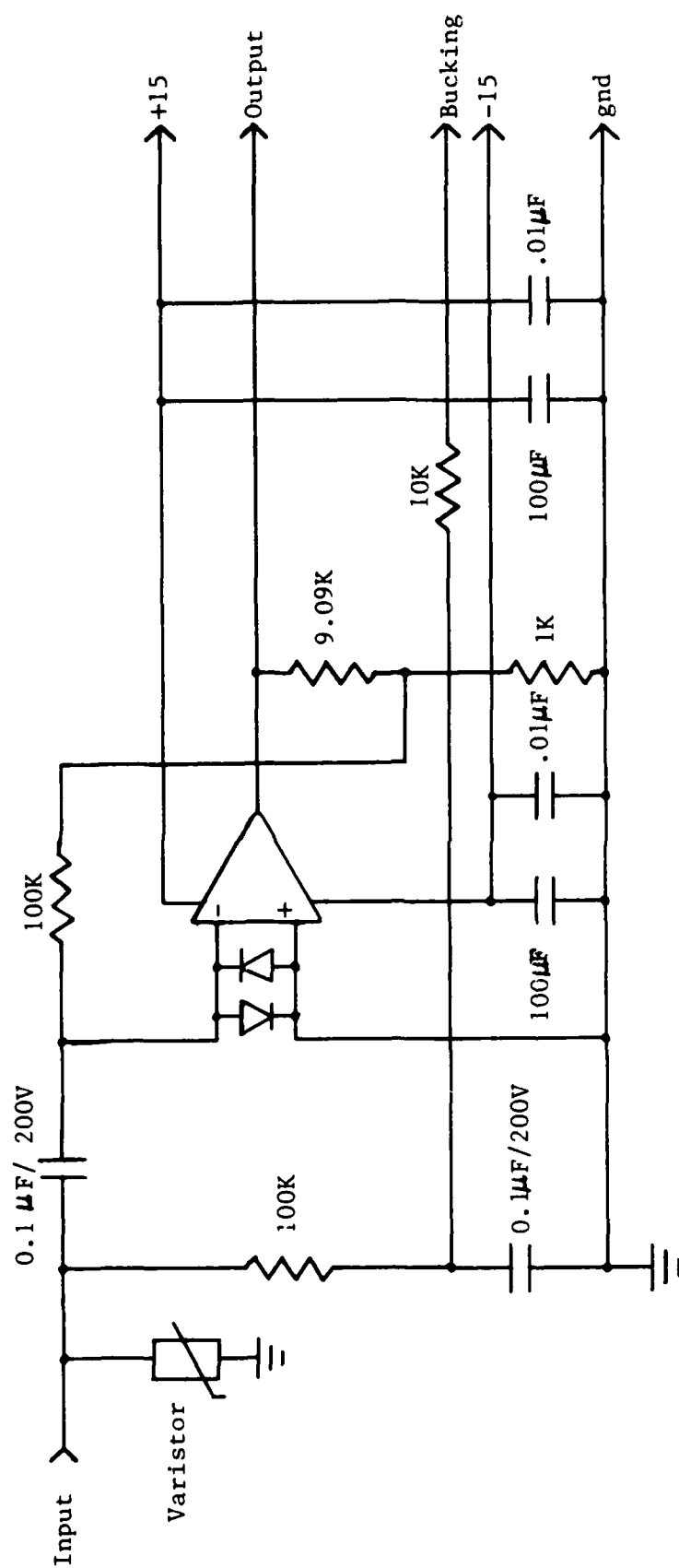
Motor shaft

Fig. 1 - Detailed drawing and photograph of field meter head.

Fig. 2 – Preamplifier schematic showing bucking voltage circuit, current mode input, protection diodes, and feedback configuration.

power leads, and has back to back diodes across its inputs to protect against surges. A DC voltage (hereafter called the bucking voltage) can be applied to the stator through this module to create an artificial field at the field meter heads for sensitivity calibration.

The rest of the amplifier (fig. 3) consisted of identical low pass filters in both the signal and reference paths, eliminating both the power frequency and signal harmonic energy. The Frequency Devices lowpass cauer-elliptic filters had a cutoff of 311 Hz chosen such that a null point occurred at the power fundamental frequency of 400 Hz. The signal was amplified and the reference path was phase shifted by a 180 degree variable half lattice phase shifter. This insured coherent phases of the signal and reference paths which were then fed into an Analog Devices synchronous demodulator (AD630KN). The demodulator has capabilities of narrow band transmission thus eliminating low frequency noise components and is followed by single pole smoothing filters for either thunderstorm ($\tau = 0.01$ sec) or calibration purposes ($\tau = 0.157$ sec). During thunderstorm flights higher time resolution was desired while during calibration the noise level was required to be minimal. The signal then passed through one final stage of DC amplification before output to the recording system.

III. RECORDING SYSTEMS

The recording systems consisted of a six channel Astro-med (W602XL) strip chart (frequency response $\simeq$ DC to 100 Hz) and a twenty channel Kyowa (RTP-602A) FM analog recorder (frequency response $\simeq$ DC to 313 Hz, S/N $\simeq$ 46 dB). The four field mill outputs were each recorded on two ranges separated by a factor of 10. A ten second slow time code provided by USAF/FDL and roll and pitch from the aircraft inertial navigation system were also recorded. The measurement of roll and pitch are critical for an accurate calibration since, especially during pitch, an accurate angle was difficult to hold. Subsequently these signals were digitized at 35 and 3.5 samples/sec for thunderstorm and calibration data respectively.
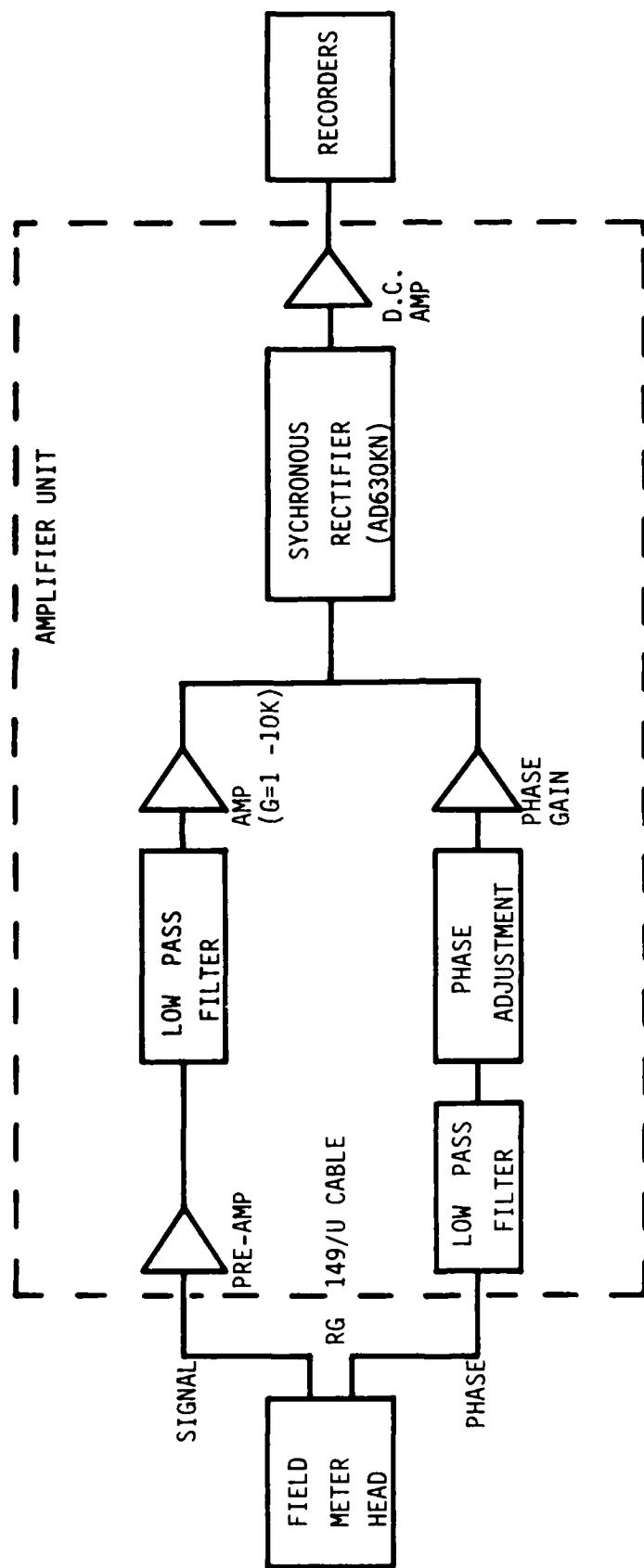
Fig. 3 – Schematic of overall field mill system showing the field meter heads, amplifiers, and recording systems.

8

IV. LOCATION AND INSTALLATION OF FIELD MILLS

Since three field components and the aircraft self charge must be meas-
ured, a minimum of four independent field mills are required. Given the
coordinate system defined in fig. 4, then a nodal curve can be defined as a
curve on the aircraft skin where one of the field component contributions is
zero and a nodal point as the intersection of two nodal curves. Optimum
locations would then be at nodal points. In principle, nodal curves could be
obtained by exposing the aircraft to a field in a particular direction and
finding the locus of points on the aircraft skin where there would be a null
response. There are three nodal curves and at least six nodal points on any
aircraft. On the CV-580 the nodal points occur near the wingtips, at the
nose and the tail, and on the top and bottom of the fuselage (fig. 5). The
simplest case is the Ey nodal curve (no response to an Ey field), which is a
locus of points along the top and bottom of the fuselage created by cutting
it with the one plane of symmetry perpendicular to the wingspan and parallel
to the fuselage. The other nodal curves and points are indicated approxi-
mately in the figure. No attempt has been made to calculate their exact
locations. Mazur et. al. [1986] have determined, with model calculations,
approximate nodal points for the NASA F-106 aircraft. The curvature of the
aircraft makes the exact locations difficult to determine.

A tail location on the rudder is impractical and a nose location may be
precluded because of particle impaction on the exposed sensor parts and the
need for a more powerful motor to overcome the increased airflow drag. The
wingtips provide good measures of both the wing to wing electric field and
the aircraft self charge. Wingtip locations provide a large field enhance-
ment factor which makes measurement of the fair weather field for calibration
purposes much easier. Model calculations have larger errors associated with
modelling the wingtip compared to fuselage locations since grid sizes are not
in general fine enough. For model calculations, reasonable locations might
be inboard on the fuselage if the shielding properties of the wings are con-
sidered. For those who want to compare model and experimental calibration
techniques, it might be appropriate to have redundancy along the wingtip axis
(two on the wingtips and two inboard). Finally, installation sites should
avoid as much as possible protrusions such as antennas, lights, and wheels
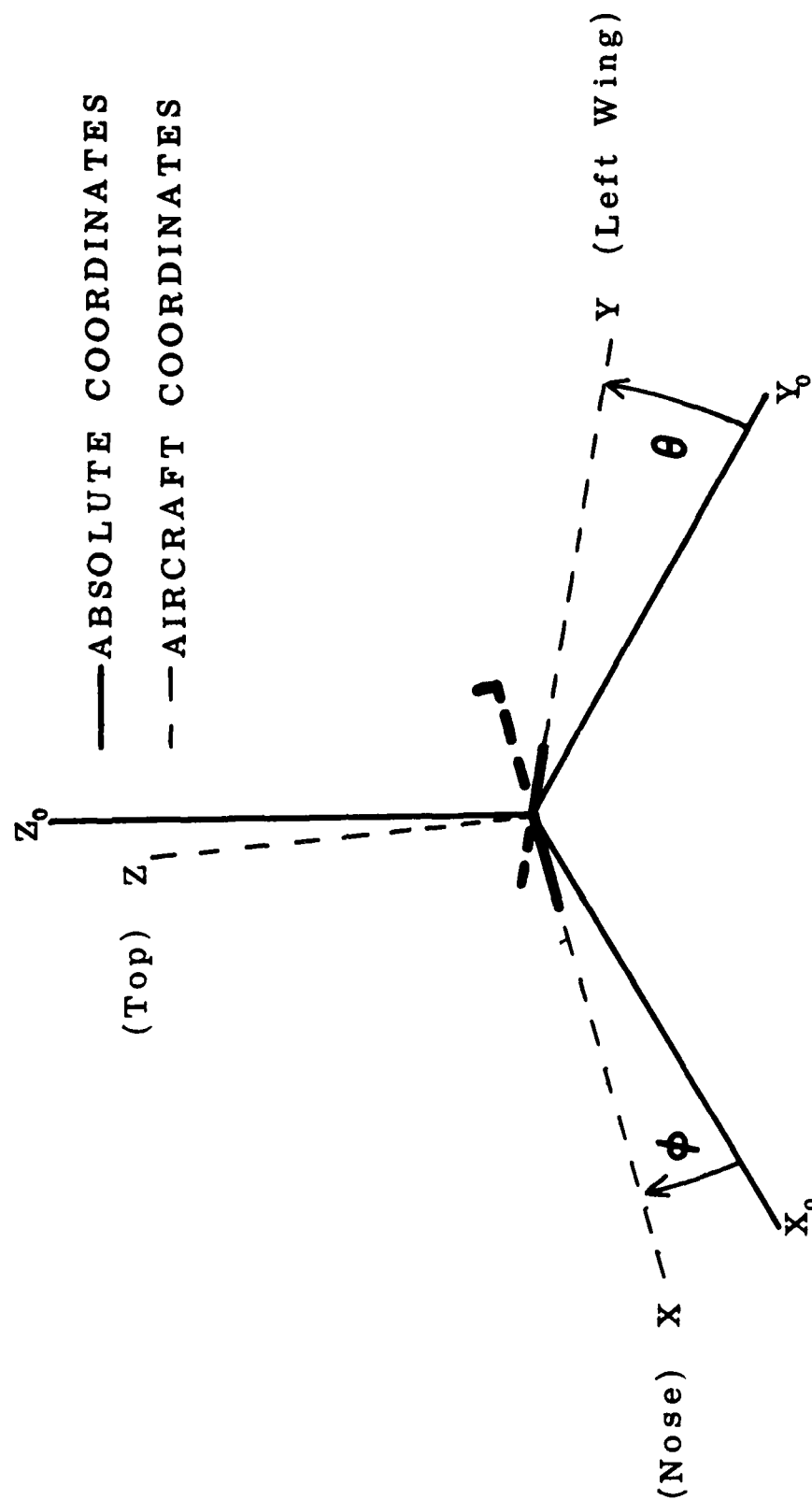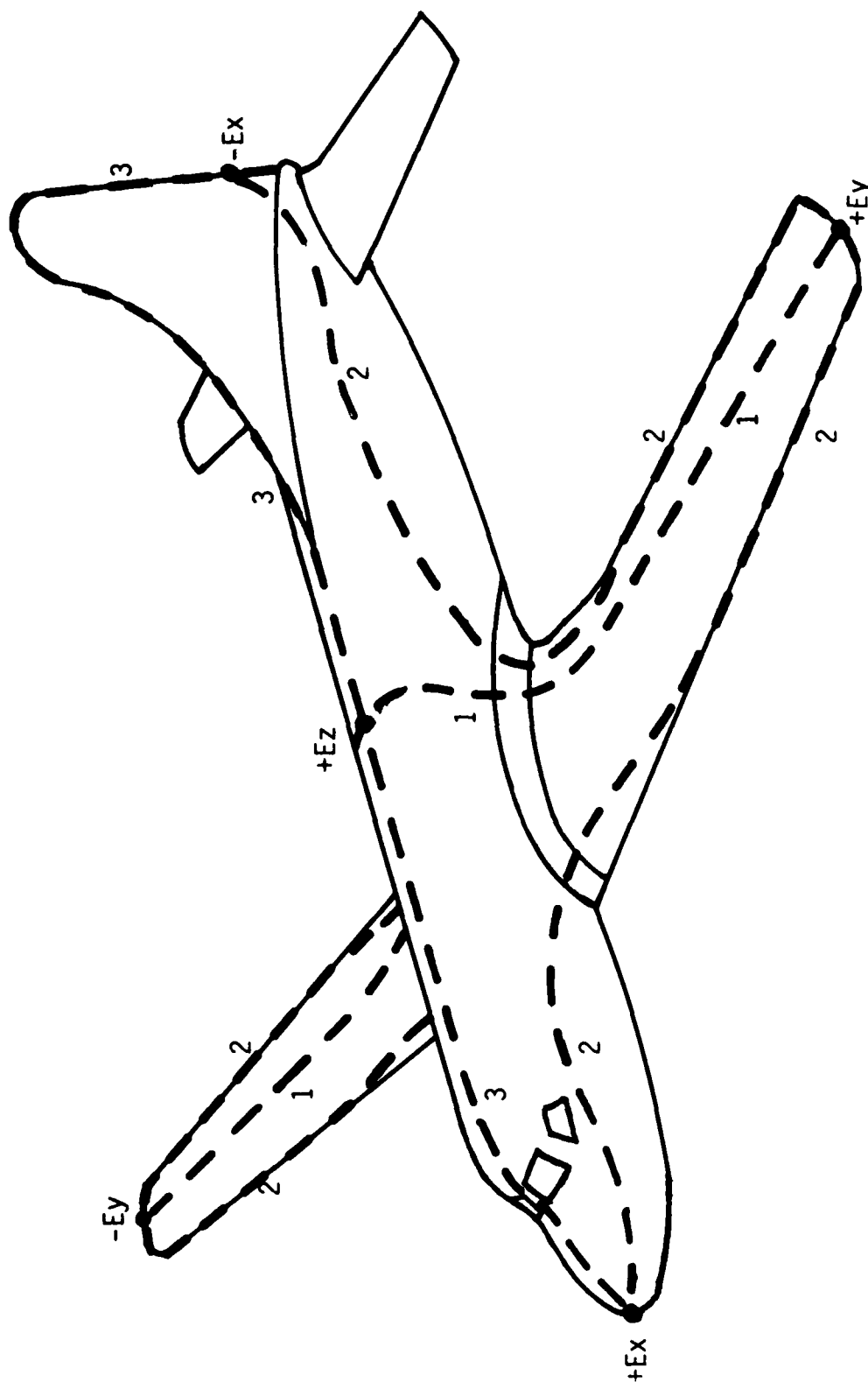which could cause shielding effects or accumulate surface charges.

Fig. 4 - Coordinate system for calibration procedure showing absolute and aircraft coordinates. Both the roll (θ) and pitch (ϕ) angles are indicated.

Fig. 5 - Approximate location of nodal curves and nodal points on CV-580 aircraft. The nodal point under the fuselage is not shown.

1 -- Ex Nodal Curve
2 -- Ey Nodal Curve
3 -- Ez Nodal Curve

11

The field meter locations on the CV-580 (fig. 6) were two mills symmetri-
cally opposed on the wingtips (approximately at nodal points) and two mills
on the belly of the fuselage (along a nodal curve), as far forward and aft,
respectively, as possible in order to maximize the separation for the nose-
to-tail field. The nose location was discarded both from the necessity of
the radar installation and from the water impaction expected during cloud
penetrations. Unfortunately, a field meter at the top of the fuselage was
not used because of the fear that it would fill with water. Subsequent ana-
lysis indicates that a field meter at this location would be valuable. In a
typical installation (fig. 7), the field meters were attached by four stain-
less steel screws which facilitated their removal. In this wingtip configur-
ation the glass light cover was sprayed with a conductive spray (Chemtronics
Static Free) during calibration flights to eliminate static charges.

V. PROBLEMS ASSOCIATED WITH FAIR WEATHER CALIBRATION

Previous experiences at NRL on the PB4-Y2, EC121K, and the S2D aircraft
indicate that with reciprocating engines the aircraft self charge was rela-
tively low. Boulay and Laroche [1982] conclude for a Gloster Meteor turbojet
aircraft little engine charging occurs. The CV-580 turboprop, however, was
found to exhibit severe charging problems such that the fair weather field
was completely masked. In order to reduce the self charge to a fairly stable
low level, .003 inch (.0762 mm) stainless steel wires [Anderson + Bailey,
1986b] were attached to the trailing edges of the ailerons (fig. 8). This
reduced the aircraft potential to the corona potential of the wicks, low
enough such that a sensitive range was reached by offsetting the remaining
self charge with a reasonable bucking voltage.

VI. CALIBRATION MATRIX THEORY

In order to discuss the details of the calibration procedure, a few defi-
nitions must be made. Given the coordinate system (fig. 4), where the air-
craft coordinates (dashed) are related to an absolute coordinate system
(solid), a system of equations describing the response of the four field mill
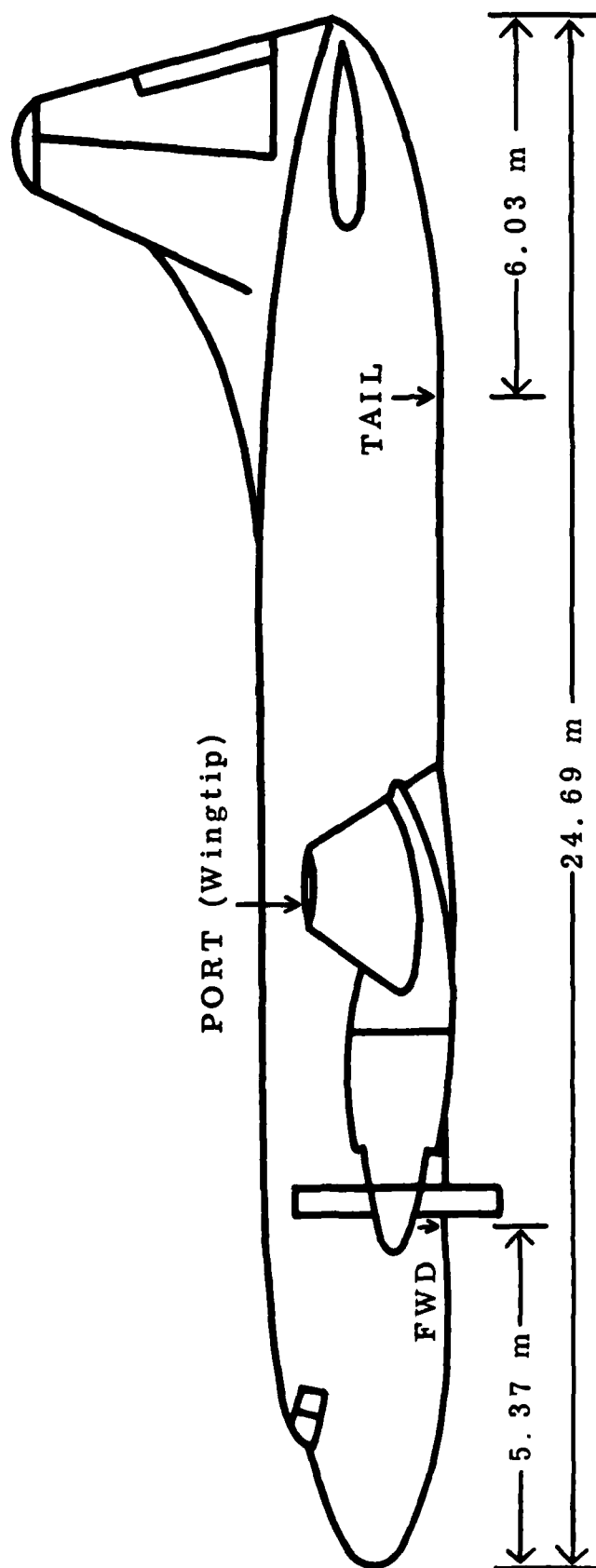system can be written as:

Fig. 6 - Location of field meters on CV-580 aircraft. The STBD meter, in the same configuration as the PORT meter, is not shown.

Stainless steel ring

Fig. 7 - Photograph of a wingtip field meter installation.
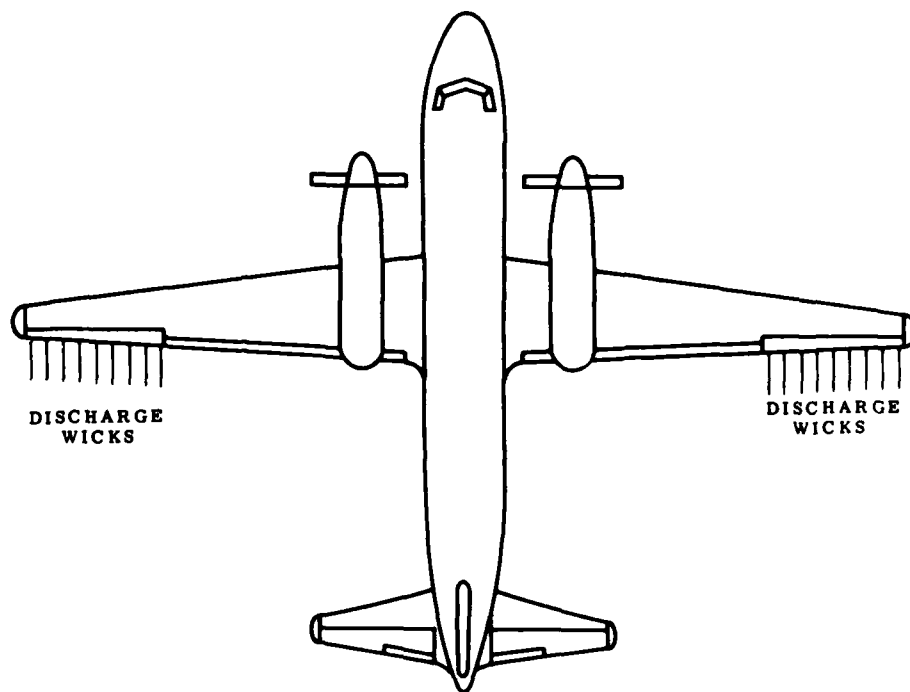
DISCHARGE
WICKS

DISCHARGE
WICKS

Fig. 8 - Attachment of stainless steel wires to the trailing edges of the
ailerons. Both the standard discharge wicks and the attached wires
are shown.

$$Ep = Px\ Ex + Py\ Ey + Pz\ Ez + Pq\ Q$$

$$Es = Sx\ Ex + Sy\ Ey + Sz\ Ez + Sq\ Q$$

$$Ef = Fx\ Ex + Fy\ Ey + Fz\ Ez + Fq\ Q \tag{1}$$

$$Et = Tx\ Ex + Ty\ Ey + Tz\ Ez + Tq\ Q$$

where Ex, Ey, Ez, and Q are the field components and the self charge with
respect to the aircraft coordinates; Ep, Es, Ef and Et are the fields at the
mill for the PORT, STBD, FORWARD (under the fuselage), and TAIL (also under
the fuselage) mills respectively; and the coefficients Px ... Tq are the
enhancement coefficients (note that they are dimensionless except for the
self charge coefficients). Symmetry considerations suggest that the wingtip
mills will respond to an Ey field with equal magnitude and opposite sign and
to the other field directions and to the self charge with equal magnitude and
same sign. Responses to Ex and Ez fields are included here because it is not
yet known how close we are to wingtip nodal points. Furthermore, the belly
mills, located on the centerline of the aircraft, should be insensitive to an
Ey field. Here we are quite certain that we are on a nodal curve since this
is the only true plane of symmetry. The matrix equations thus reduce to:

$$Ep = Px\ Ex + Py\ Ey + Pz\ Ez + Pq\ Q$$

$$Es = Px\ Ex - Py\ Ey + Pz\ Ez + Pq\ Q$$

$$Ef = Fx\ Ex \qquad\quad + Fz\ Ez + Fq\ Q \tag{2}$$

$$Et = Tx\ Ex \qquad\quad + Tz\ Ez + Tq\ Q$$

In order to take advantage of the wingtip symmetry, it is convenient to
derive and record the two quantities:

$$Y \equiv (Ep - Es)/2 = Py\ Ey \tag{3}$$

$$Q^` \equiv (Ep + Es)/2 = Px\ Ex + Pz\ Ez + Pq\ Q \tag{4}$$

which give a direct measure of both Ey and self charge (it turns out that $Q^`$
is only slightly contaminated by the Ex and Ez fields). In the enhancement
matrix above it is assumed that the coefficients are statistically indepen-
dent and the vectors are linearly independent.

The external fields and the self charge are obtained by inverting the matrix. The results are the following:

$$Ex = \frac{\left\{\dfrac{FqTz}{Pq} - \dfrac{TqFz}{Pq}\right\}\left\{\dfrac{Ep + Es}{2}\right\} + \left\{\dfrac{TqPz}{Pq} - Tz\right\}Ef + \left\{Fz - \dfrac{FqPz}{Pq}\right\}Et}{\text{COMMON DENOMINATOR}} \quad (5)$$

$$Ey = \frac{(Ep - Es)}{2\,Py} \quad (6)$$

$$Ez = \frac{\left\{\dfrac{TqFx}{Pq} - \dfrac{FqTx}{Pq}\right\}\left\{\dfrac{Ep + Es}{2}\right\} + \left\{Tx - \dfrac{TqPx}{Pq}\right\}Ef + \left\{\dfrac{FqPx}{Pq} - Fx\right\}Et}{\text{COMMON DENOMINATOR}} \quad (7)$$

$$Q = \frac{(FzTx - FxTz)\left\{\dfrac{Ep + Es}{2}\right\} + (PxTz - PzTx)Ef + (PzFx - PxFz)Et}{Pq * \text{COMMON DENOMINATOR}} \quad (8)$$

where COMMON DENOMINATOR is given by

$$\frac{FqPxTz}{Pq} - \frac{TqPxFz}{Pq} + \frac{TqPzFx}{Pq} - \frac{FqPzTx}{Pq} + FzTx - FxTz$$

Note that the field components depend only on ratios of the self charge coefficients while the self charge depends on the absolute values. While the vectors of the inverted matrix composed of the above equations are linearly independent the individual coefficients are now statistically dependent. This dependence will affect the error analysis seen in section VIII.

VII. DETERMINATION OF ENHANCEMENT COEFFICIENTS

The determination of the enhancement coefficients can logically be divided into separate determinations of field and self charge coefficients. Furthermore each set contains one arbitrarily chosen absolute coefficient (we choose Py and Pq) to which the others can be expressed as ratios.

A. Self charge coefficients

Once a sensitive enough range is attained, then the ratio of the self
charge coefficients can be determined through changes in the self charge
brought about by varying the engine characteristics (e.g. - varying rpm or
power) or by traversing small non-electrified cloud tufts which charge the
aircraft by waterdrop impaction. For the CV-580 the charging by water impac-
tion was opposite in sign compared to the engine charging. An example of
charge variation is given in figure 9 where the engine power was varied
sequentially from cruise power to low power (600 HP) to high power (2500 HP).
Apparently cruise power and high power produce approximately the same char-
ging rate on the CV-580. This may be caused by the corona wires limiting the
maximum aircraft potential. The mixing techniques as discussed in section
VII.C can be used as an alternative method of determining these ratios.

To determine the absolute self charge coefficient Pq, comparisons must be
made between in flight and ground measurements. The effects of image charges
as the aircraft approaches the ground cause artificial enhancement of the Pq
coefficient. Ground measurements of the fields observed upon the application
of a known DC voltage to the aircraft, while the wheels were resting on bases
of 1/4 inch (6.35 mm) plywood and 1/16 inch (1.59 mm) electrically insulating
polyethylene mats, were performed at Patuxent Naval Air Station. The ratio
of the measured field to the known DC voltage relates aircraft potential to
the field in the presence of the image aircraft. The effect of the image can
be evaluated from examination of data recordings taken during the landing
process. Immediately prior to touchdown, the image is identical to that seen
on the insulating mats. Since the self charge was dominant during the
landing approaches, field variations can be ignored. Thus Pv, in terms of
the equivalent voltage produced by Q, can be defined for the PORT (p) mill
as:

$$Pv \equiv (Epa/Va) = (Epa/Epl)*(Epl/Vl)*(Vl/Va) \qquad (9)$$

where Epa, Epl, Va, and Vl are the fields at the mill and potentials far
above the ground (where image charges are negligible) at altitude (a) and
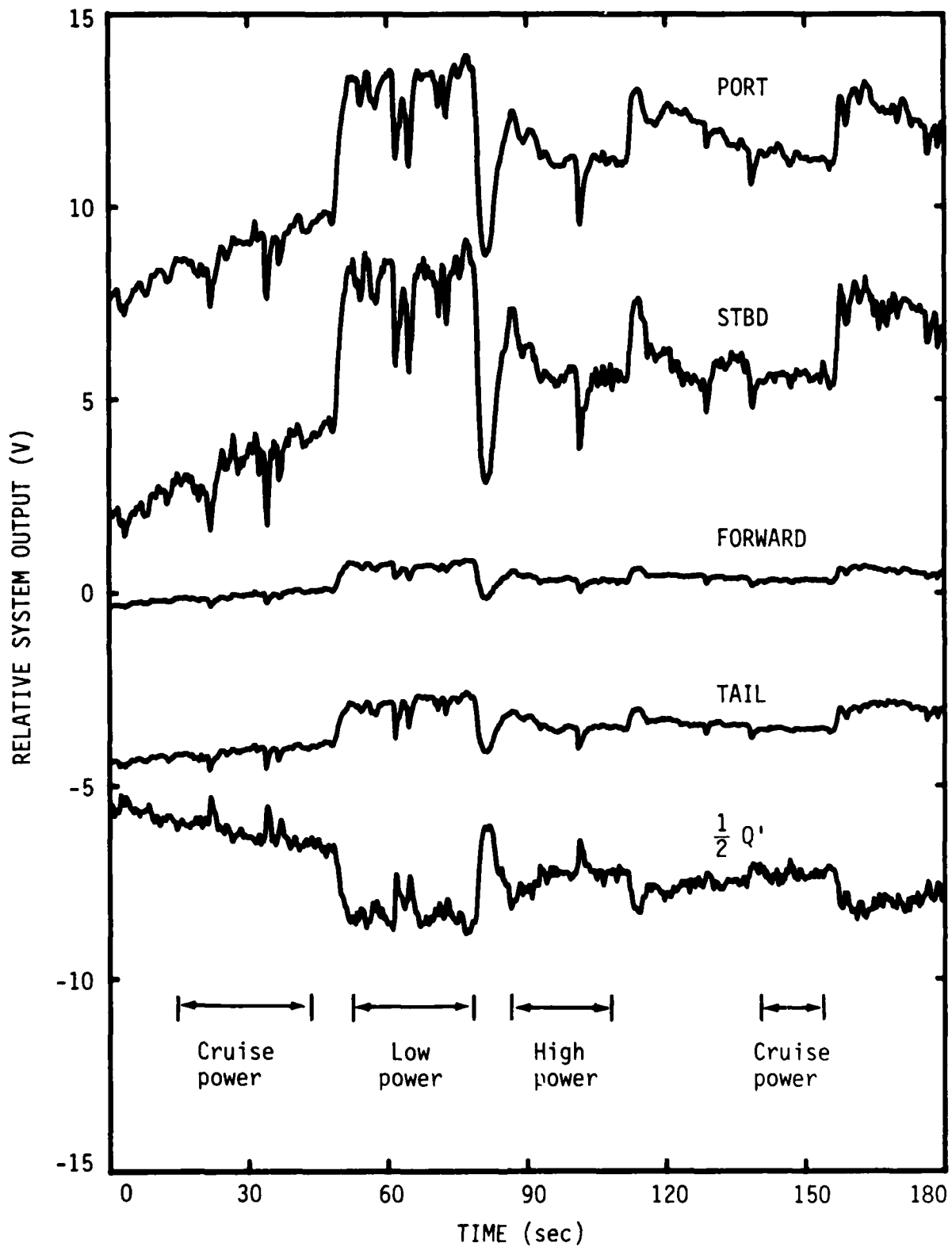just before landing (l). Assuming that the self charge Q is conserved during

18

Fig. 9 - Self charge variations induced by engine power settings during straight and level flight.

a landing approach (fig. 10), then not only is (Epa/Epl) a valid measurement, but we have the following additional result:

$$Q = Ca \; Va = Cl \; Vl \tag{10}$$

where Ca and Cl are the capacitances in air and at landing. The Patuxent ground measurements on the insulated mats yield (Epg/Vg) which is assumed to be identical to (Epl/Vl), where Epg is the field at the mill produced by the DC voltage Vg. Thus Pv becomes:

$$Pv = (Epa/Epl)*(Epg/Vg)*(Ca/Cl) \tag{11}$$

Note that Pv instead of Pq has been found (Pq Q and Pv V are equivalent).

The capacitance ratio Ca/Cl can be determined by modeling of the aircraft. An expression for the capacitance of a conducting sphere above an infinite conducting plane has been derived [Morse + Feshbach, 1953]. It is obvious that the sphere underestimates the true capacitance of an aircraft at small heights. Another simple model which should overestimate the capacitance of the aircraft at small heights is a circular disc parallel to a ground plane [Andersen, 1983]. At small heights, it is possible to use the parallel plate formula for capacitance with little error; while the capacitance of the disk at infinite height is available in analytic form [Terman, 1943]. The capacitance variation with height for the sphere and disk models is plotted in fig. 11 normalized to the values at infinite height. Both sphere and disk were assigned a radius of 6.76 meters which gives the same horizontal cross sectional area as the CV-580 aircraft. The aircraft height above the ground at the lowest point on the bottom of the fuselage of 1.54 meters is indicated in figure 11 by the arrow and nearly coincides with the intersection point of the two models. The capacitance ratio at this intersection point is 0.54.

As noted earlier, a value for Pv has been obtained. Pq is available if an absolute aircraft capacitance is known. Pv, which relates self charge field to voltage on the aircraft, is certainly a useful quantity; but Pq could be estimated from the 752 pF capacitance at infinity of a sphere of
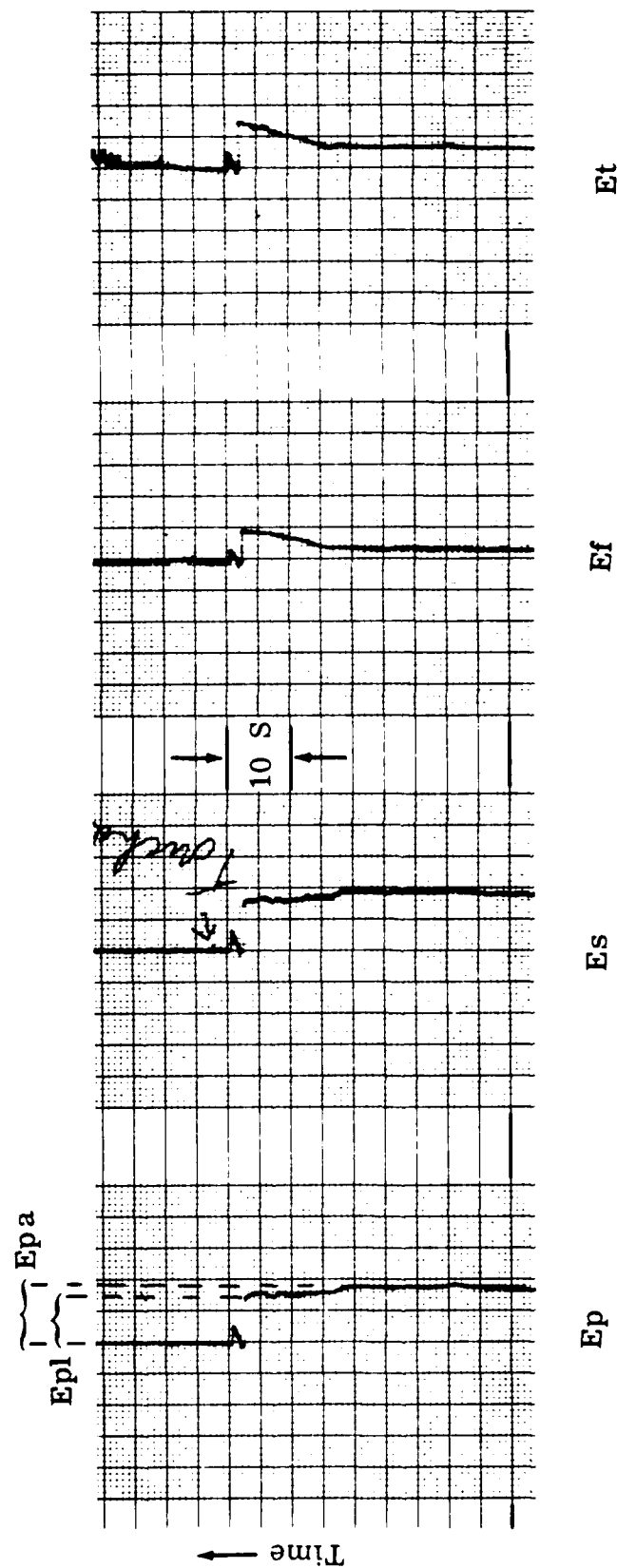
20

Fig. 10 - Typical data recording obtained during landing showing the effect of the electrostatic image of the aircraft on the measured fields approaching and at touchdown.
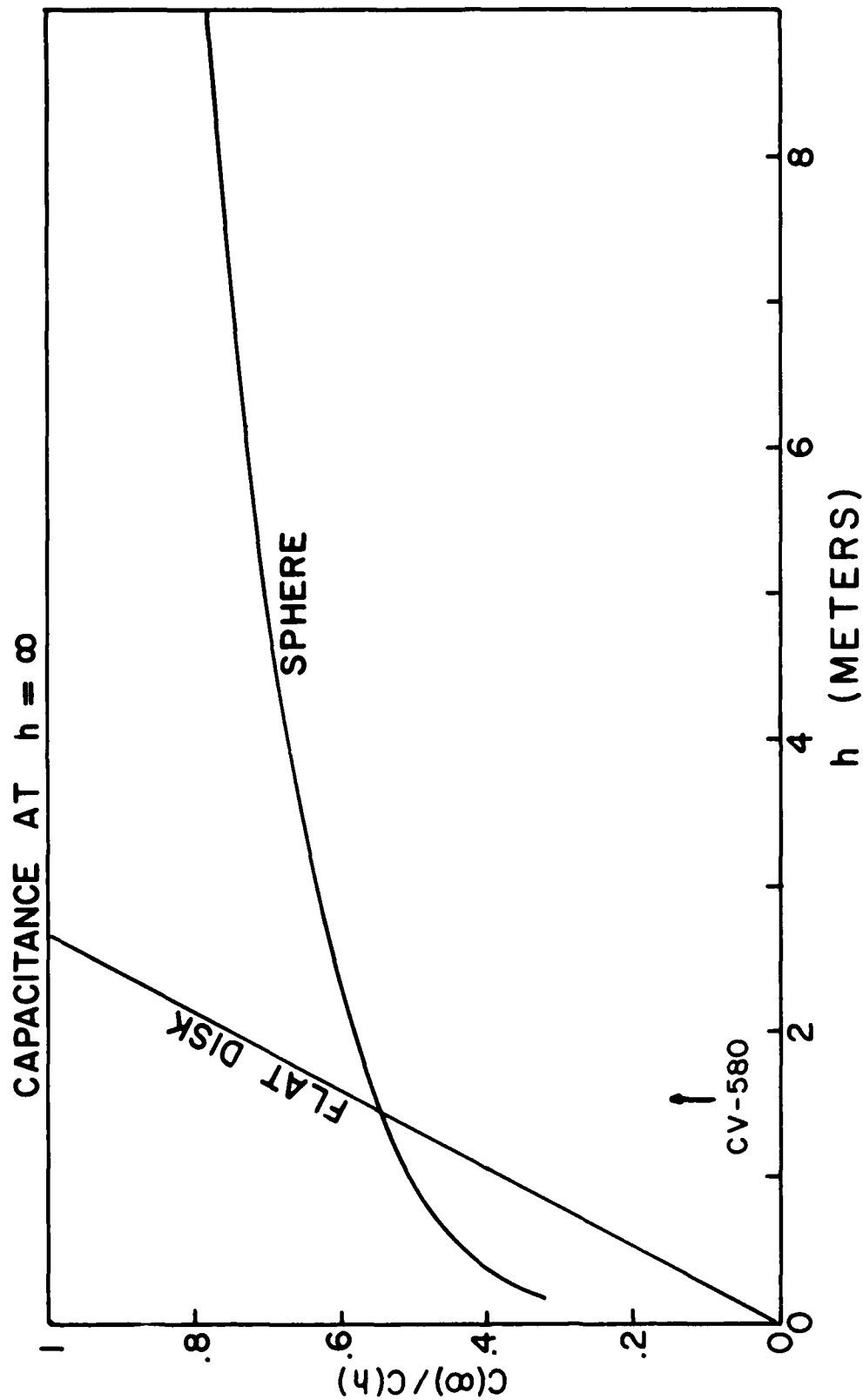
21

Fig. 11 - Normalized capacitance values for conducting sphere and circular disk as functions of height. The height (1.54 m) of the lowest point on the underside of the CV-580 fuselage is indicated.

22

6.76 meter radius (this estimate is probably high - the disk model gives a value of 479 pF). The measured values for each factor in equation 11 are:

$$Epg/Vg = 2.044 \ (V/m)/V$$
$$Epa/Epl = 1.273$$

and

$$Ca/Cl = 0.54$$

which yields

$$Pv = 1.41 \ (V/m)/V$$

Corresponding values for Pq (= Pv/Ca) would be 1875 $(V/m)/\mu C$ (C=752) or 2944 $(V/m)/\mu C$ (C=479) where a realistic value might be the mean value of 2410 $(V/m)/\mu C$. The overall error of Pv is determined from the error of each factor above. Epg/Vg is known accurately ($<$ 3%) while the error on the capacitance is difficult to ascertain. The capacitance ratio Ca/Cl is fairly well known. This is why we calculate Pv instead of Pq. The biggest error term will probably be the measurement of Epa/Epl.

Note that a distinction should be made between Cl (just before touchdown) and Cg (sitting on the ground). Cg was also measured over a concrete ramp at Patuxent with a value of 3010 pF. Given the capacitance ratio of Ca/Cl = 0.54 and the estimates from the models for Ca then it is found that Cl has the limits of 887 to 1393 pF which is a factor of two to three different from Cg. The difference is probably due to the distortion of the tires when sitting on the ground which lowers the aircraft and provides a larger footprint of the wheels. Both effects tend to increase the measured capacitance.

B. Absolute field coefficient Py

With the instrumentation on this aircraft and because of the .igh self charge it must be pointed out that the fair weather field can only be measured by difference techniques (either the field must change quickly or aircraft maneuvers must be performed); therefore, comparisons with a ground site were not practical. This leaves two options of absolute calibration: 1) direct comparison with an aircraft calibrated to measure the vertical field or 2) the profile technique where a known value is assumed for the

ionospheric potential. The profiling technique is defined by measuring the field at regular altitudes from near ground height to the ceiling limits of the aircraft. These measurements can then be approximately integrated to obtain the ionospheric potential. A direct comparison with another aircraft requires close formation flying. It can eliminate the need for quickly covering multiple altitudes but has the distinct disadvantages of relying on another aircraft calibration and on the coordination of aircraft positions and communication between two research groups. The profile technique must be done quickly and depends critically on the weather conditions.

During direct comparisons, Airborne Research Associates' Baron aircraft, instrumented with four radioactive potential probes (two on each wing separated vertically by 1.45 m), performed joint maneuvers with the CV-580. The Baron's calibration is based on low level passes over an instrumented ground site. Its accuracy is probably between 5 and 10 percent. Since this is lower than our calculated Py uncertainty it cannot be a major factor in our overall uncertainty. Also, spatial errors in the fields, due to the aircrafts occupying different airspaces, are probably much larger. The Baron's contribution was essentially to measure the vertical fair weather field while the CV-580 did rolls.

Given a vertical fair weather field E, during a roll maneuver θ (positive for right banks - see fig. 4) an Ey field appears from zero as:

$$Ey = E \sin(\theta)$$

therefore Py can be calculated from left and right banks as

$$Py = \frac{Y(\theta_1) - Y(\theta_2)}{E (\sin(\theta_1) - \sin(\theta_2))} \tag{12}$$

Normally θ_1 and θ_2 are nominally either $\pm$ 30 or $\pm$ 45 degrees respectively. Since the angle of roll varies somewhat during each maneuver, it is probably better to divide each point within the roll by its appropriate angle, average, and then difference with the values in the other angle. E is obtained easily from the other comparison aircraft.

24

For the profile technique, an uncalibrated measurement of the vertical field must be integrated with respect to height h to the ionsphere yielding a value for the ionospheric potential. Py can be calculated from:

$$Py = \frac{\int [Y(\theta_1) - Y(\theta_2)] \, dh}{V (\sin(\theta_1) - \sin(\theta_2))} \tag{13}$$

where the ionospheric potential V has been previously measured. Since the aircraft has limits on both the lowest and highest altitudes of flight, a typical profile (fig. 12) must be extrapolated to both the ground and the ionosphere. The ground field was assumed to be the same as the lowest measurement (200 ft.) while the ionosphere value is corrected by the slope above the inversion level (exponential tail). The apparent vertical potential plotted on top in figure 12 is the quantity Py V. The true ionospheric potential was calculated from a compilation of yearly ionospheric potential (fig. 13) by Markson [1985]. Eliminating the three outlier points around year 1960, the mean is 246 KV ± 7%. The value of Py V must be corrected for the well known diurnal variations as expressed by the Carnegie curve (fig. 14) [Ault and Mauchly, 1926] [Whipple, 1929]. Four profiles were accomplished during the summers of 1983 and 1984 over the ocean off the coasts of Cape Canaveral, Florida and Atlantic City, N. J.

Systematic differences might exist between the direct comparison and the profile technique. The low altitude calibration of the Baron aircraft could have possible problems of image charge effects. Furthermore, altitude and airflow variations might cause distortion of the ion plumes from the radioactive potential probes thus affecting the enhancement coefficient. The profile technique has uncertainties in the assumed value of the ionospheric potential, problems with accepting diurnal variations on a daily basis, and errors in the extrapolations to both the ground and the ionosphere. Problems common to both techniques are errors in reading the data recordings, uncertainties in the altitude and attitude of the aircraft, nonstationarity of the fair weather field, and spatial inhomogeneities. In figure 15, where the profile and direct comparison are compared, a histogram of Py shows no significant differences. Py was calculated from this data set as 26.5 ± 14.2%.

PROFILE OF 08/12/85

APPARENT VERTICAL POTENTIAL (MV)

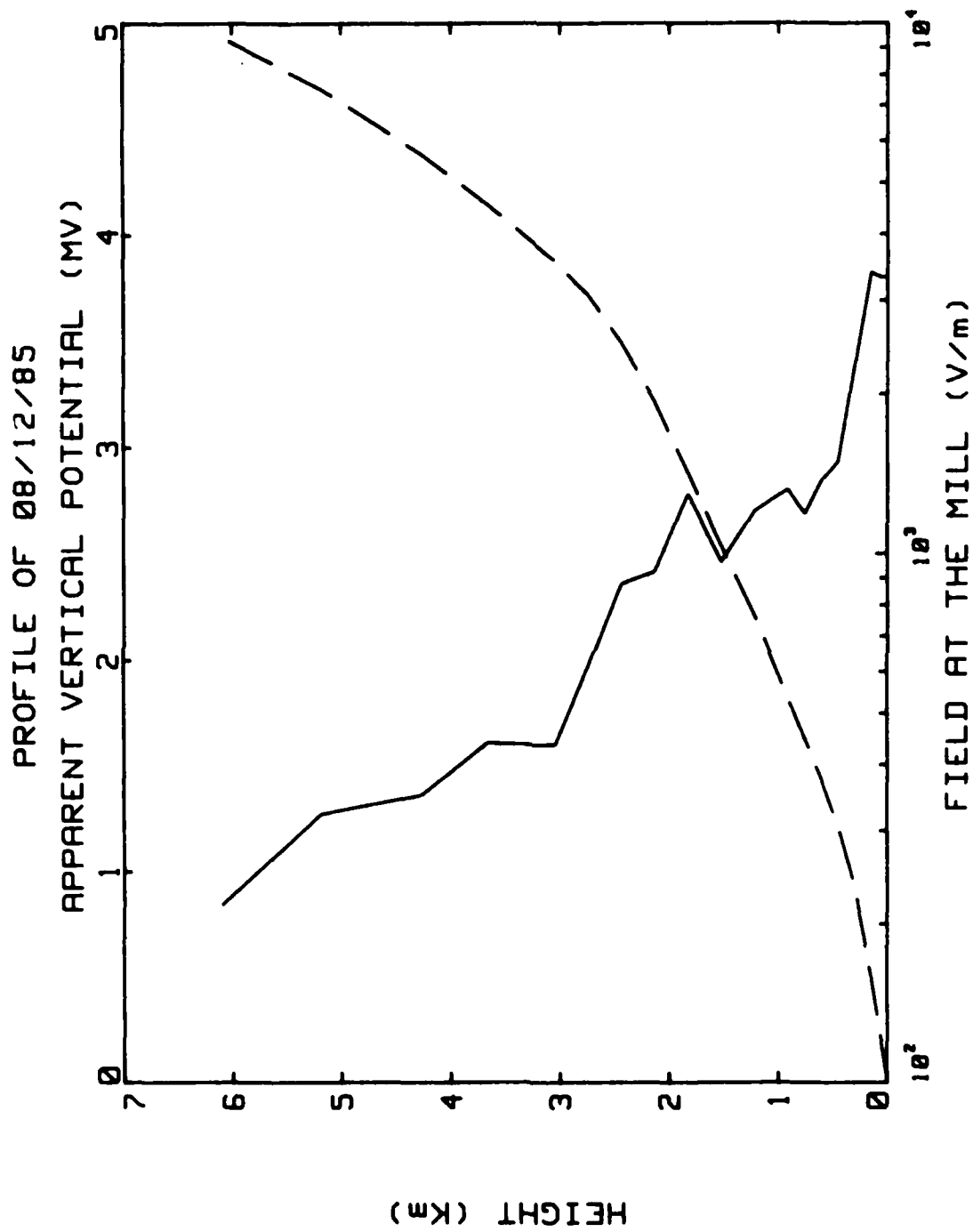HEIGHT (Km)

FIELD AT THE MILL (V/m)

Fig. 12 - Typical profile showing both the field at the mill (solid) and the apparent vertical potential (dashed).

26

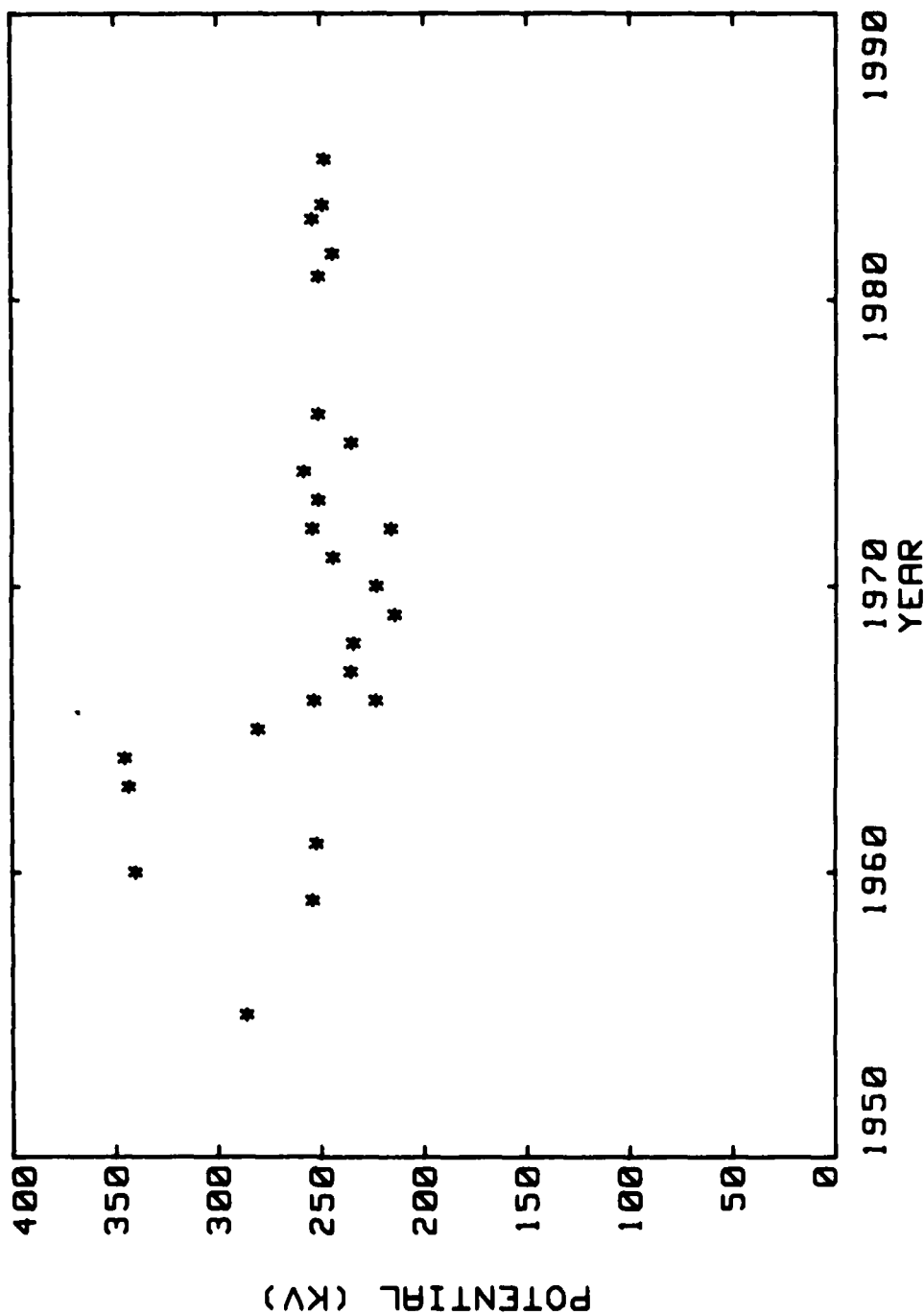YEARLY IONOSPHERIC POTENTIAL (ADAPTED FROM MARKSON)

Fig. 13 - Yearly ionospheric potential between the years 1955 to 1984 (adapted from Markson).
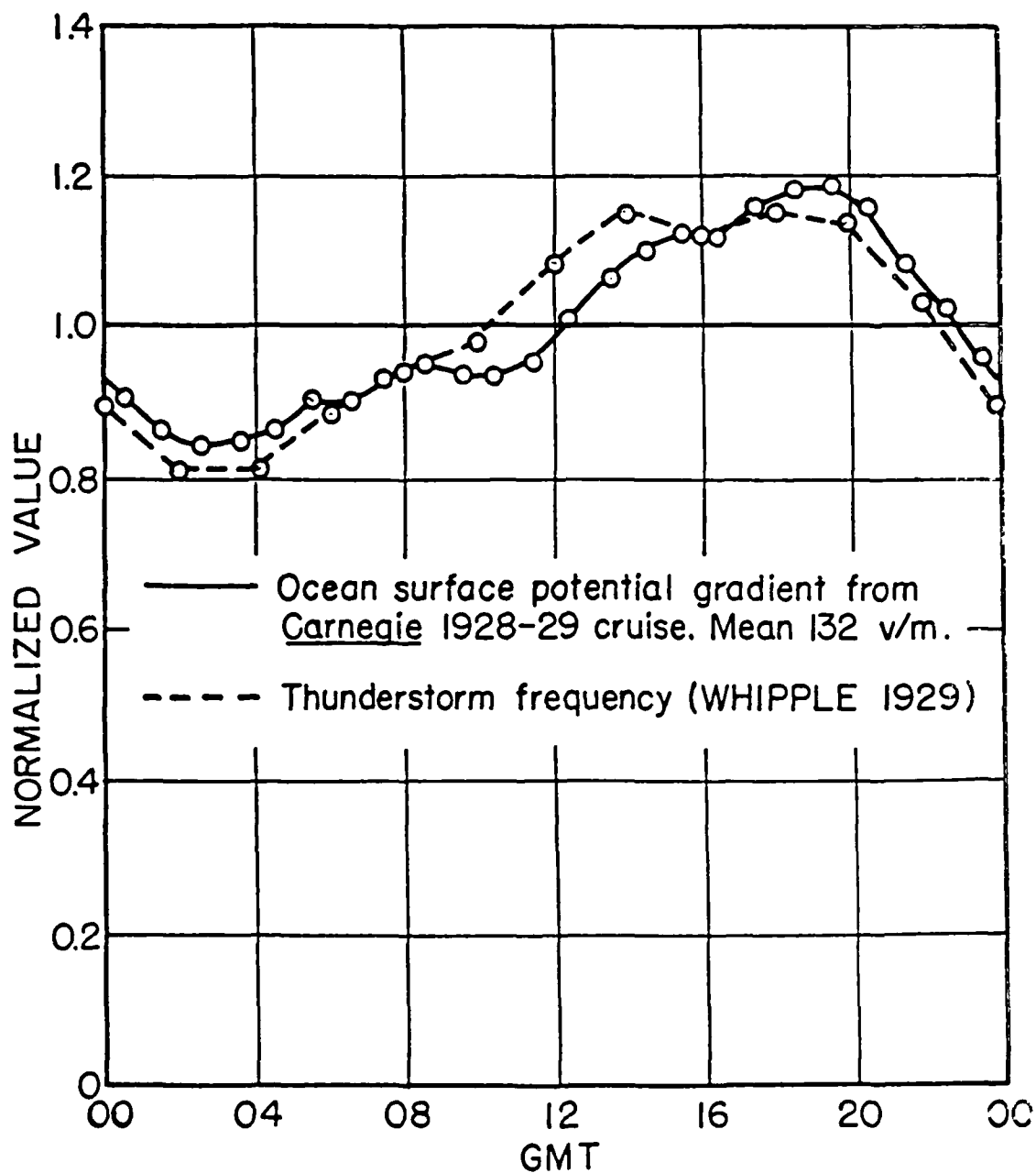
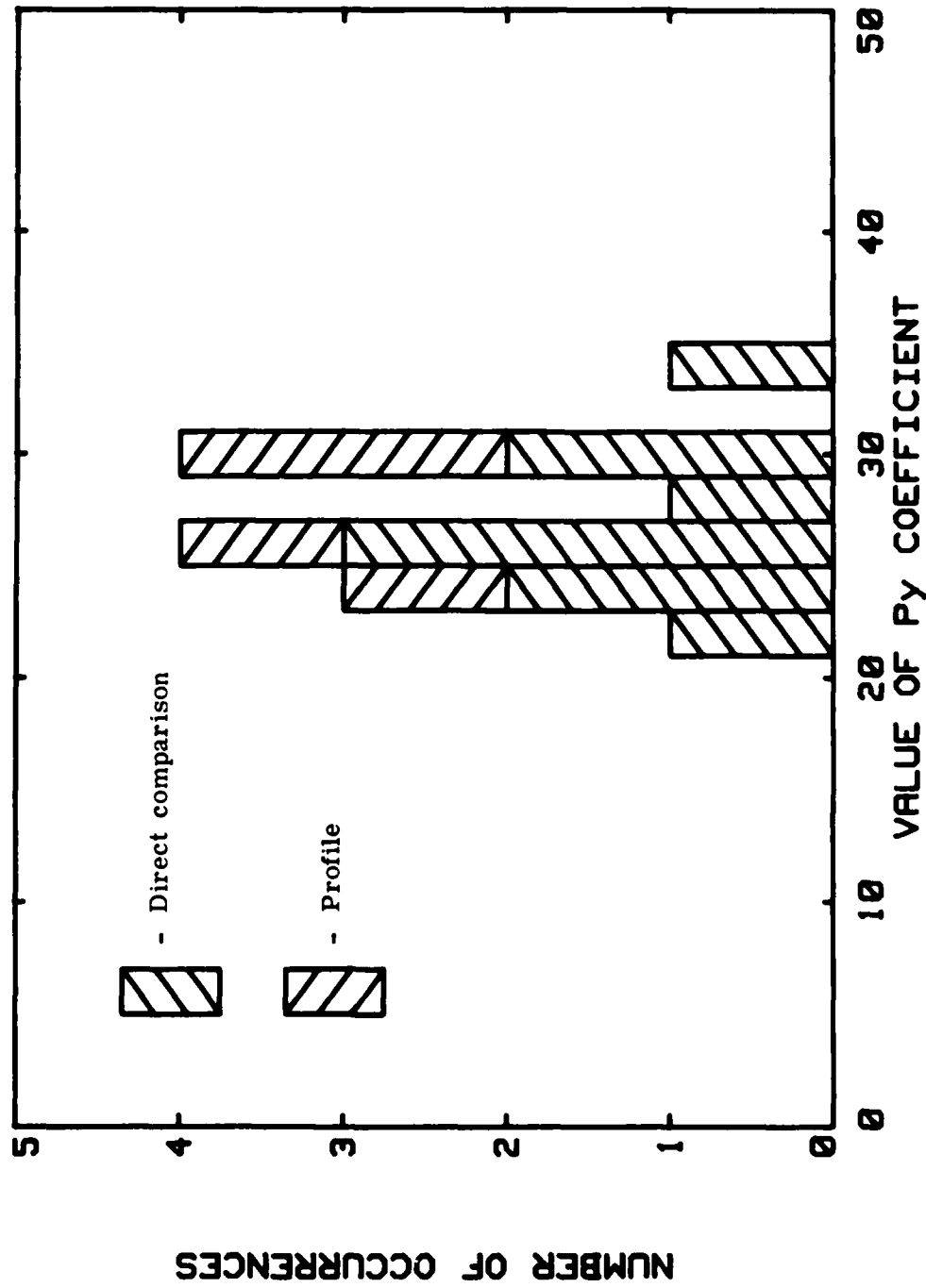Fig. 14 - Diurnal variation of ionospheric potential (Carnegie curve).

Fig. 15 - Histogram of absolute Py coefficient. The profile and direct comparison methods are indicated (see text).

C. Field ratio coefficients

This section deals with calculating the other field coefficients from the knowledge of Py. It should be pointed out that for determining the ratio of, for example, Py/Fz, the absolute fair weather field E need not be known. In this section, however, it is assumed that Py is already known, thus, E can be determined from roll but not pitch maneuvers. In calculating the ratios, some error causes will be eliminated. There will be no errors with respect to diurnal corrections, value of the ionospheric potential, and extrapolations. Remaining errors are due to non-stationarity and inhomogeneity of the fair weather field, uncertainties in attitude, changes in altitude during pitch maneuvers, and statistical fluctuations in the data (mostly due to self charge variations).

Due to the symmetry in the wingtips, the measurement of the derived Ey field is uncontaminated by self charge variations. For the belly mills and the derived quantity Q`, techniques must be devised to eliminate the more severe contamination from self charge variations. All the field coefficients except Py are affected. A high correlation exists between Q`, mostly a measure of self charge, and both of the belly mills. The mixing of the self charge as measured by Q` into the belly mills takes advantage of this correlation by largely eliminating self charge from the belly mills. By choosing mixing parameters α and β such that known self charge variations vanish, the belly mills are redefined as:

$$Ef` \equiv Ef - \alpha\, Q` = (Fx - \alpha\, Px)Ex + (Fz - \alpha\, Pz)Ez \qquad (14)$$

$$Et` \equiv Et - \beta\, Q` = (Tx - \beta\, Px)Ex + (Tz - \beta\, Pz)Ez \qquad (15)$$

where the contaminations due to Px, and Pz are left to be estimated (it will be shown later that Px and Pz are close to zero). The values for α and β were 0.149 and 0.258 respectively. As mentioned earlier, these values can be used to calculate the ratio of the self charge coefficients.

Each of the belly mill enhancement coefficients can be determined from a specific maneuver. Fz and Tz are determined from roll maneuvers while Fx and Tx are determined from pitch maneuvers. Since pitch maneuvers cannot measure

E, a set of roll-pitch maneuvers must be performed sequentially. The normal procedures were a period of straight and level flight followed by consecutive 45 degree left and right banks, another period of straight and level, a series of consecutive climb-dives ($\pm$ 15 degree), a third period of straight and level, consecutive 45 degree left and right banks, and a final period of straight and level. This allows E to be calculated during the rolls for use in the climb-dive maneuvers. With the above expressions for the belly mills uncontaminated by self charge, the four coefficients Fx, Fz, Tx, and Tz can be determined as:

$$Fz - \alpha \, Pz \; = \; \frac{Ef'(\theta) - Ef'(0)}{E \, (\cos\theta - 1)} \tag{16}$$

$$Tz - \beta \, Pz \; = \; \frac{Et'(\theta) - Et'(0)}{E \, (\cos\theta - 1)} \tag{17}$$

$$Fx - \alpha \, Px \; = \; \frac{Ef'(\phi_1) - Ef'(\phi_2)}{E \, (\sin\phi_1 - \sin\phi_2)} \tag{18}$$

$$Tx - \beta \, Px \; = \; \frac{Et'(\phi_1) - Et'(\phi_2)}{E \, (\sin\phi_1 - \sin\phi_2)} \tag{19}$$

where ϕ is the pitch angle. Note that $\pm$ 15 degree pitch angles are better than 30 degree dives since they can be performed in sequences, less altitude variation occurs, the pilots are more willing to perform them, and the relative change is greater (2 sin15 $>$ sin30).

The mixing techniques described above are illustrated in fig. 16-19 for the Fx, Tx, Fz, and Tz coefficients. The improvement in the data quality is clearly evident when the top (Q' not removed) is compared to the bottom plot (Q' removed). The data traces, at least for Fx, Tx, and Fz (fig. 16-18) do exactly what is expected. Roll maneuvers for the belly mills will produce a reduction in the voltage seen by the mill in both a left and right bank (due to the evenness of the cosine function). Pitch maneuvers, on the other hand, will produce a sinusoidal behavior depending on whether a climb or a dive is being performed. The changes seen in the Fx and Tx traces should be of opposite polarity while the changes in the Fz and Tz traces should be of same polarity.
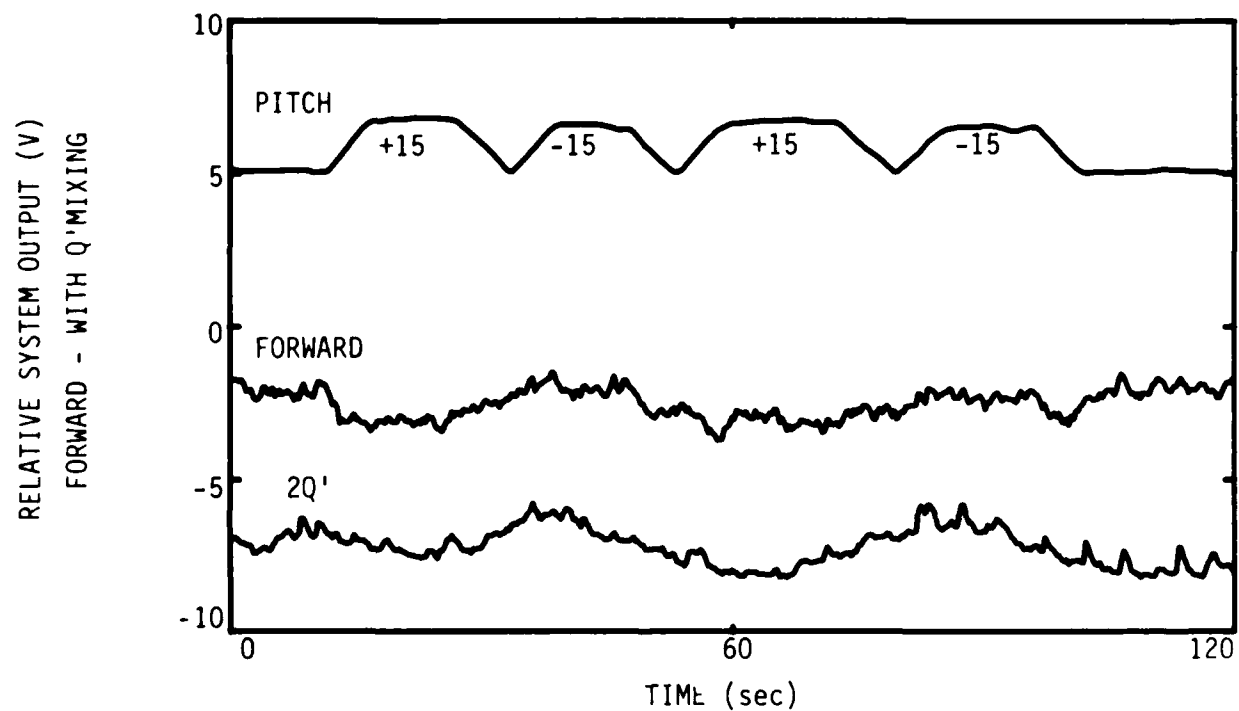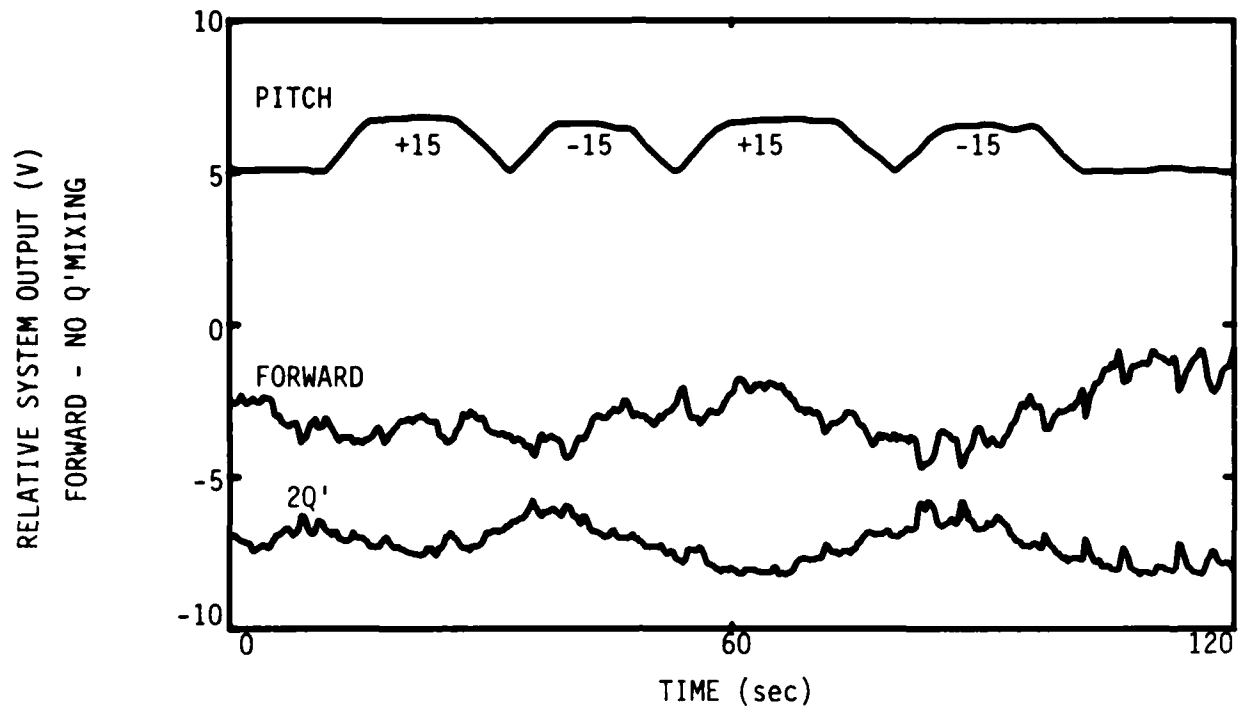
Fig. 16 - Fx coefficient - mixing of Q` into FORWARD mill during climb-dives to minimize Q variations (top - no mixing, bottom - with mixing).

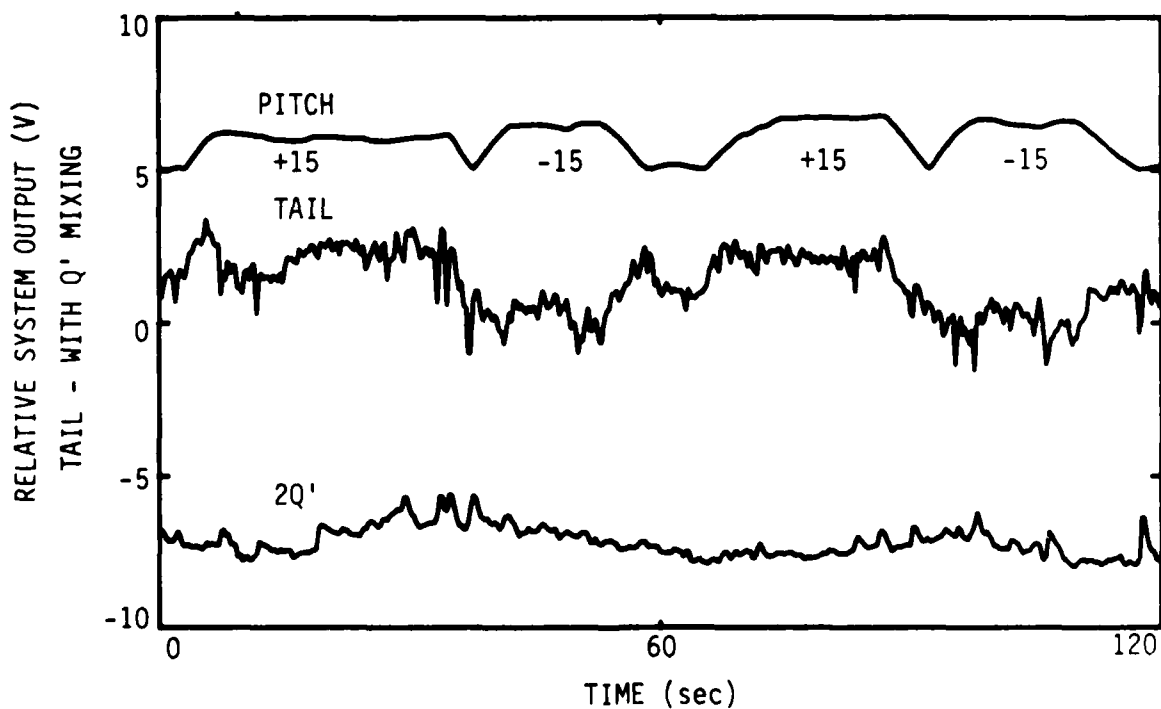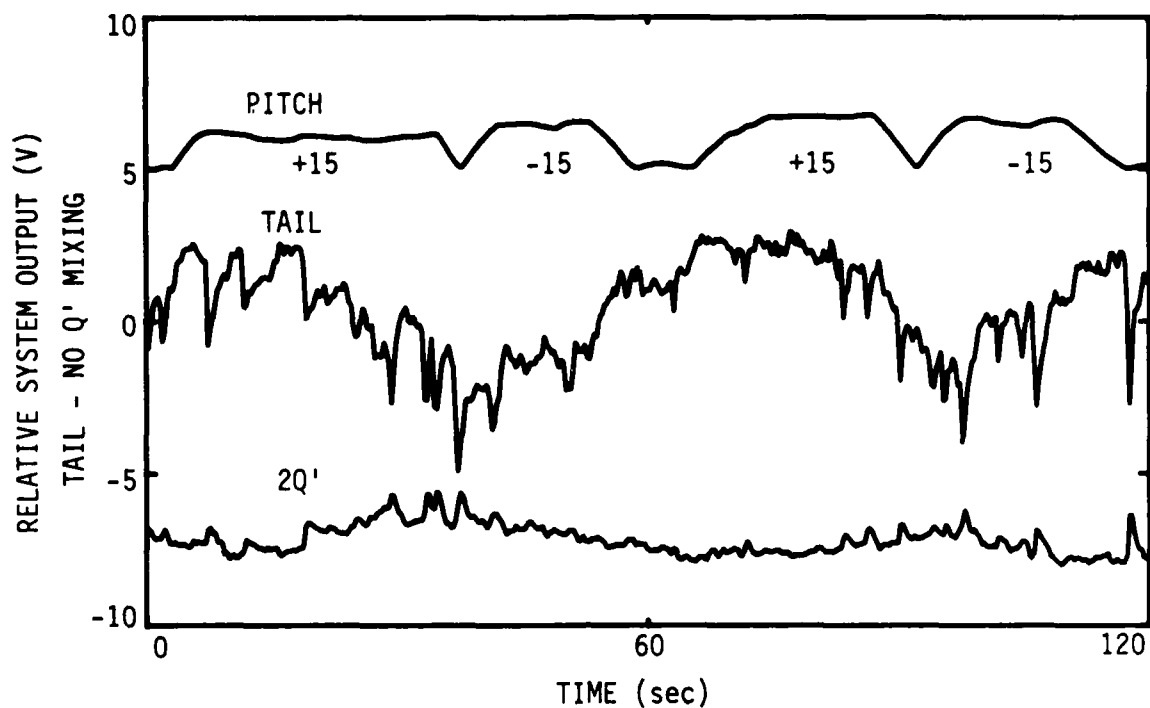CALIBRATION FLIGHT (08/12/85)

Fig. 17 - Tx coefficient - mixing of Q` into TAIL mill during climb-dives to
minimize Q variations (top - no mixing, bottom - with mixing).
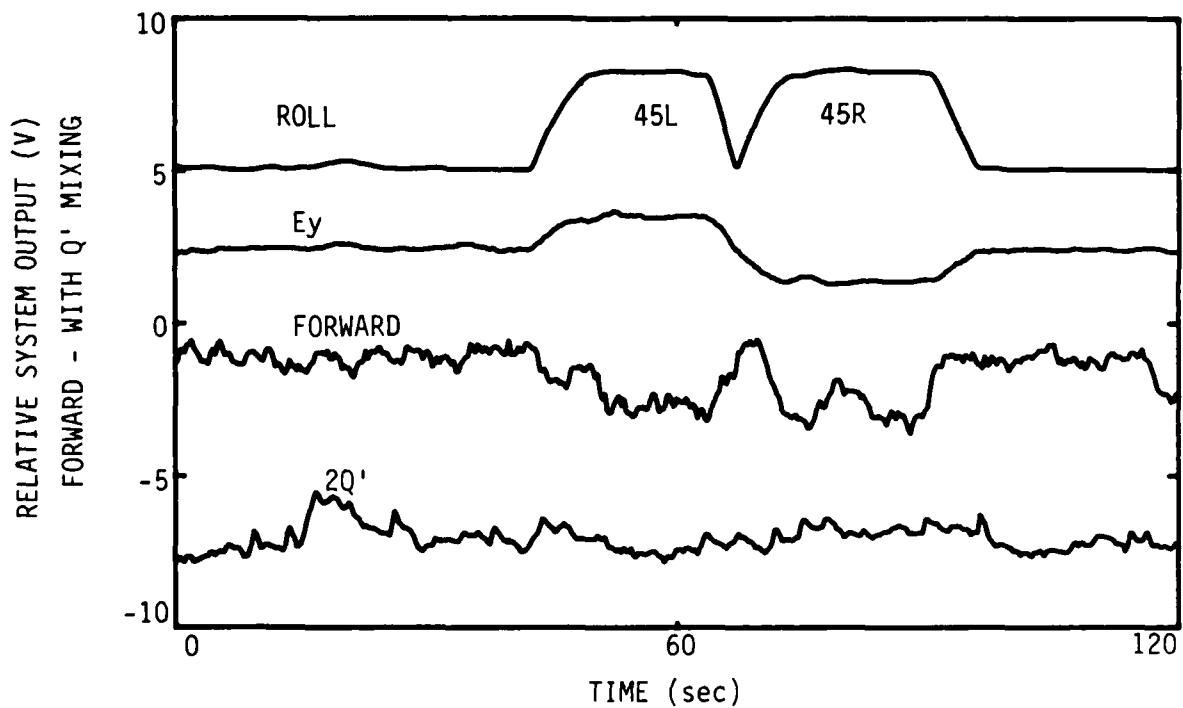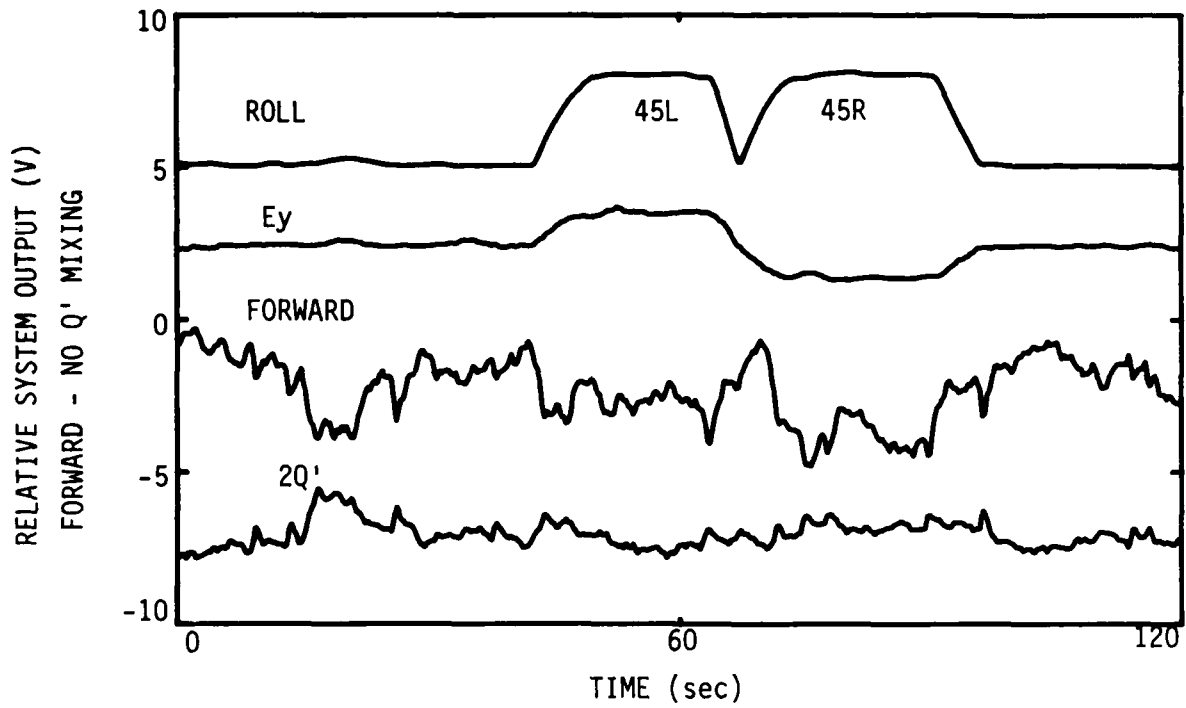
CALIBRATION FLIGHT (08/12/85)

Fig. 18 - Fz coefficient - mixing of Q` into FORWARD mill during rolls to
minimize Q variations (top - no mixing, bottom - with mixing).
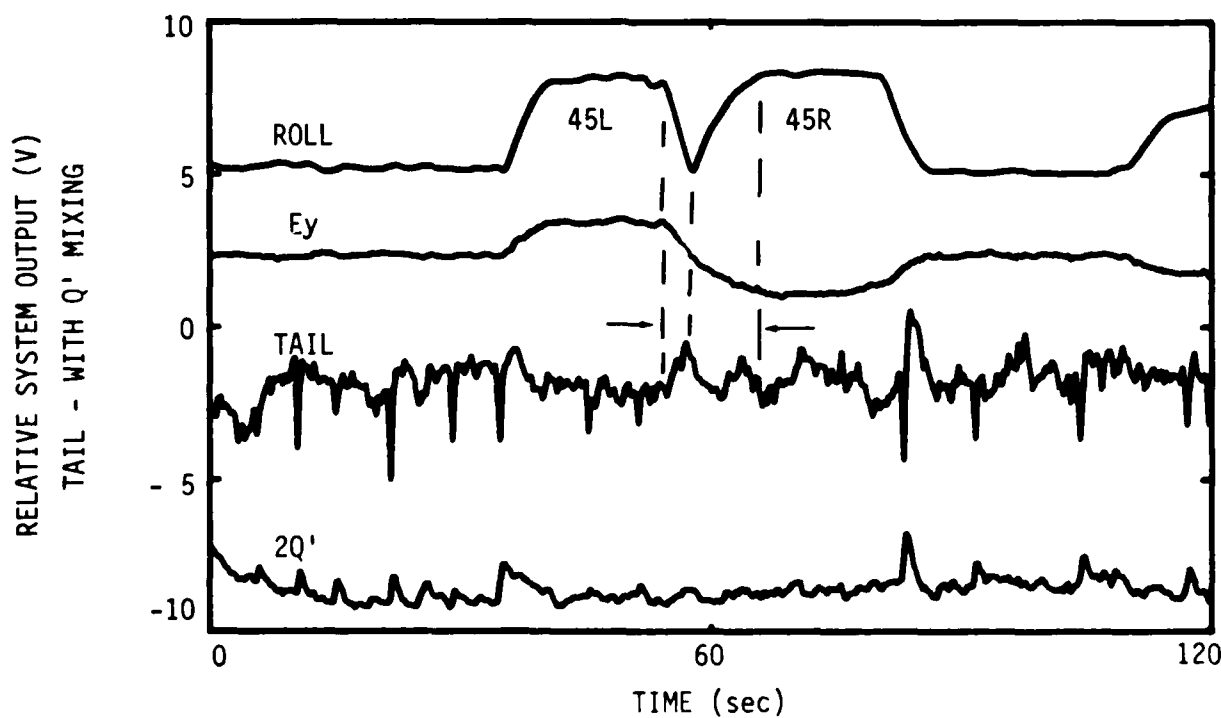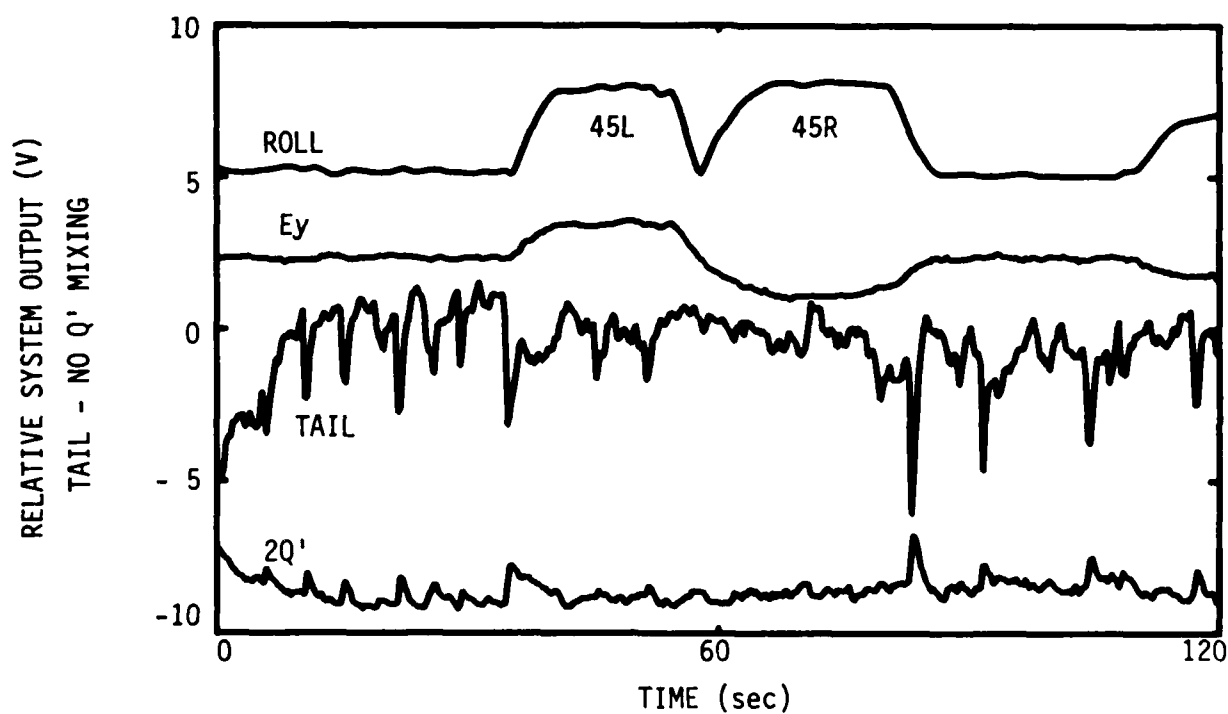
Fig. 19 - Tz coefficient - mixing of Q` into TAIL mill during rolls to minimize Q variations (top - no mixing, bottom - with mixing). Because of the poorer data quality, the region used for the analysis is indicated (see text).

35

As can be seen from fig. 19, the measurement for the Tz coefficient is not readily apparent. Apparently, for this case, either the self charge removal was inadequate or the signal is inherently noisier due perhaps to space charge plumes emitted from the engines drifting past the TAIL meter. Since good quality traces over the time of the roll maneuver were not easily identifiable, the data analyzed was the small region (as indicated) between the left and right banks as the roll angle passes through straight and level. Even with this approach, many traces were still unusable, therefore, two criteria were adopted. Since Q variations are evidently very important, in the first criterion, cases were chosen such that no severe changes in Q` occurred during the short period of time of the indicated measurement region. The second criterion, requiring equivalent amplitudes on both sides of the straight and level after a return to the 45 degree angle, helps eliminate linear trends.

Other than the suggestion of the exhaust plumes, there is no apparent reason as to why the measurement of Tz should be bad. There is a factor of approximately 2 reduction in the change in signal seen in a pitch versus a roll maneuver (2 sin15 vs. cos45 - 1); however, the same roll maneuver gives reasonable results for the FORWARD mill. Also, the same TAIL mill, during a pitch maneuver gives accurate results for the Tx coefficient. It is also reasonable to assume that the value obtained for Tz should be close to the value obtained for Fz. As is seen later, this is indeed borne out. Therefore, even though the data quality is suspect, the value obtained appears to be about what would be expected.

The values of both the Px and the Pz coefficients must be known to eliminate their contamination in the above calculations. In order to measure these coefficients, we must examine the derived quantity Q` (eq. 4), which measures mostly self charge, during both roll and pitch maneuvers. In principle, Px and Pz can be determined from pitch and roll maneuvers in a similar manner as Fx, Tx, Fz, and Tz from:

$$Px = \frac{Q`(\phi_1) - Q`(\phi_2)}{E (\sin\phi_1 - \sin\phi_2)} \qquad (20)$$

$$Pz = \frac{Q`(\theta) - Q`(0)}{E (\cos\theta - 1)} \qquad (21)$$

36

Unfortunately Q is strongly contaminated. An independent measure of the self charge is required. Fortunately, since during fair weather there is only a field component (E) in the vertical direction, a combination of the FORWARD and TAIL mills, now with some knowledge of the belly mill coefficients, gives the required independent measure. For instance during a pitch maneuver the FORWARD and TAIL mill responses are:

$$Ef = (Fx \sin\phi + Fz \cos\phi)E + Fq\ Q \tag{22}$$

$$Et = (Tx \sin\phi + Tz \cos\phi)E + Tq\ Q \tag{23}$$

Solving these equations for Q gives:

$$Q = \frac{(Tx \sin\phi + Tz \cos\phi)Ef - (Fx \sin\phi + Fz \cos\phi)Et}{(Fq\ Tx - Tq\ Fx)\sin\phi + (Fq\ Tz - Tq\ Fz)\cos\phi} \tag{24}$$

Unfortunately, since Tz and Fz are the same sign, this equation for Q gives inaccurate results since the denominator for small angles (FqTz - TqFz) is close to zero. The result is the near elimination of Q along with E from equations 22 and 23, where Q is what was to be calculated. The above solution essentially differences two mills that are on the same side of a nodal curve (Ez direction) where it is difficult to separate the effect of the self charge and the field contribution. Better mill placement would be similar to the wingtip mills, which are symmetrically on opposite sides of the Ey nodal curve. Since the belly mills are on opposite sides of the Ex nodal curve, then fields in only the x direction can effectively be eliminated (e.g. - terms involving FxEt and TxEf). In this case, the two field coefficients Fx and Tx are now opposite in sign. The result is:

$$Q = \frac{Tx\ Ef - Fx\ Et + (Fx\ Tz - Tx\ Fz)\cos\phi\ Ez}{Tx\ Fq - Fx\ Tq} \tag{25}$$

The last term is kept since, even though it is small compared to Q, it is of the same order of magnitude as the coefficient (in this case Px) being measured. If the angles of pitch are the same on both sides (i.e. - ± 15 degrees) then for the pitch case the last term will cancel. For roll maneuvers, a belly mill should be differenced with a mill on top of the fuselage. Since no such mill is available, a similar approach as with the pitch maneuvers is taken. The result is the same as equation 25 except that ϕ is replaced by θ. Since, according to eq. 21, the comparison is made between

37

banks and level flight, the last term cannot be dropped. Typical examples of
the elimination of the self charge from Q` are shown in figures 20 and 21.
Each figure shows both Q` (top) and Q`-PqQ (bottom), where Q is found from
equation 25. In the data analysis further corrections have been made to
compensate for linear trends. We can now substitute Q`-Pq in place of Q`
into eqs. 20 and 21 to find Px and Pz. Now that values for Px and Pz are
known, their contamination in the belly coefficients can be eliminated.

Some further discussion is warranted on the trends in Q that appear
during climb-dive maneuvers (fig. 20). They are not due to a real measure-
ment of Px since the variations fail to align with the pitch angle (there
appears to be some phase offset). Also they can easily be identified as self
charge variations from the independent belly mill measurements. Apparently
the self charge on the aircraft is always corona limited. Rates of corona
discharge are sensitive to airspeed, pressure, humidity, temperature, and the
absolute magnitude and direction of the external field. A simple model of
the sensitivity of the corona discharge for an isolated point in space under
quasi-static conditions, considering airspeed only, has been developed
[Chalmers, 1967]:

$$i_c = A \, V \, w \tag{26}$$

where i_c, A, V, and w are the corona discharge current, proportionality con-
stant, aircraft potential, and airspeed, respectively. Here the assumptions
have been made that the engines maintain a constant charging current and self
charge variations are caused only by the corona wires. Determining the air-
speed simply from gravitational acceleration and ignoring drag, a solution
for the shape of V can be found:

$$V = \frac{i_c}{A \, (w_0 + g \int \sin(\phi(t) - \phi_0) \, dt)} \tag{27}$$

where w_0 = 90.1 m/s (175 Kts) is the aircraft cruising speed, g is the gravi-
tational constant, and ϕ_0 = +3.5° is the cruising pitch angle. A simple
check on the validity of the results predicted by this formula can be made by
examining the airspeed. The maximum (157 m/s = 305 Kts) and minimum (66.5
m/s = 129 Kts), as derived from the data, should not greatly exceed the red-
line (250 Kts at low altitude) and stall (90 - 95 Kts) speeds for the air-
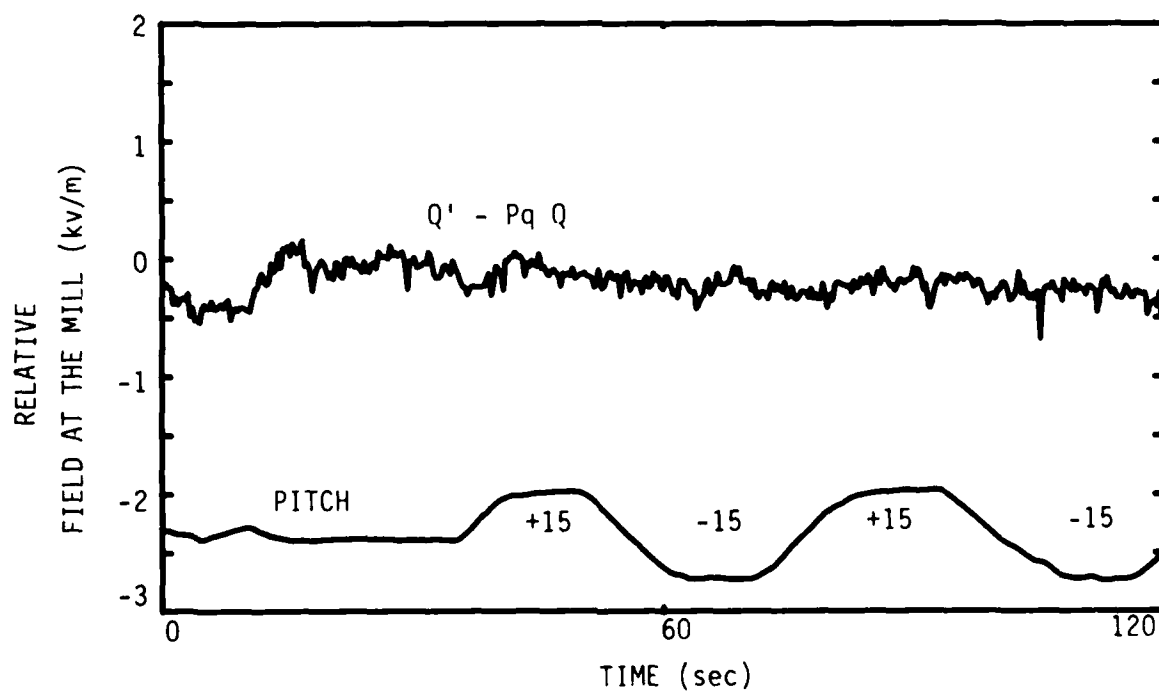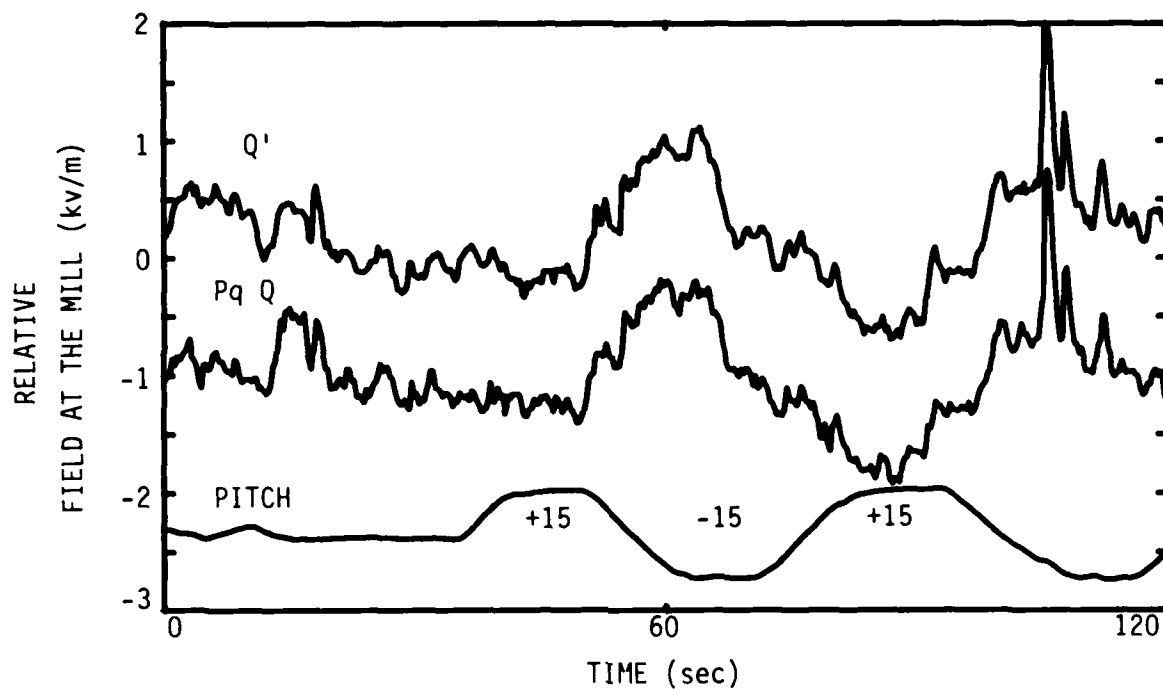craft. Since the drag term has been ignored these values are probably

38

Fig. 20 - Px coefficient - subtracting Pq Q as measured independently from the FORWARD and TAIL mills during pitch maneuvers (see text).
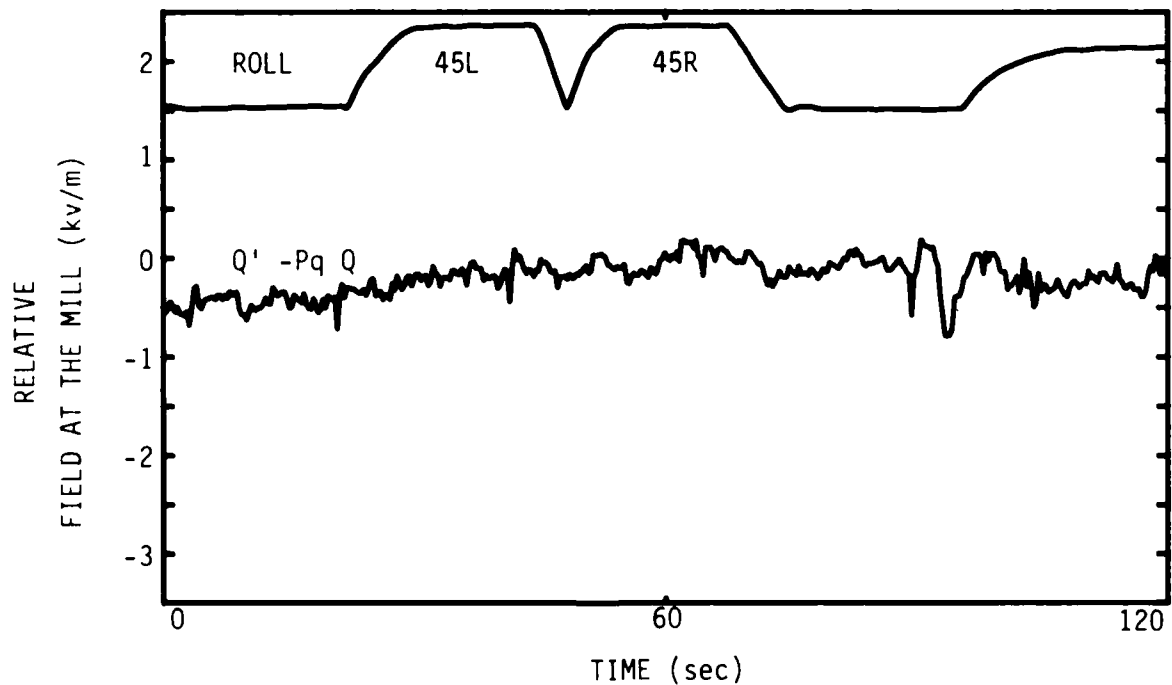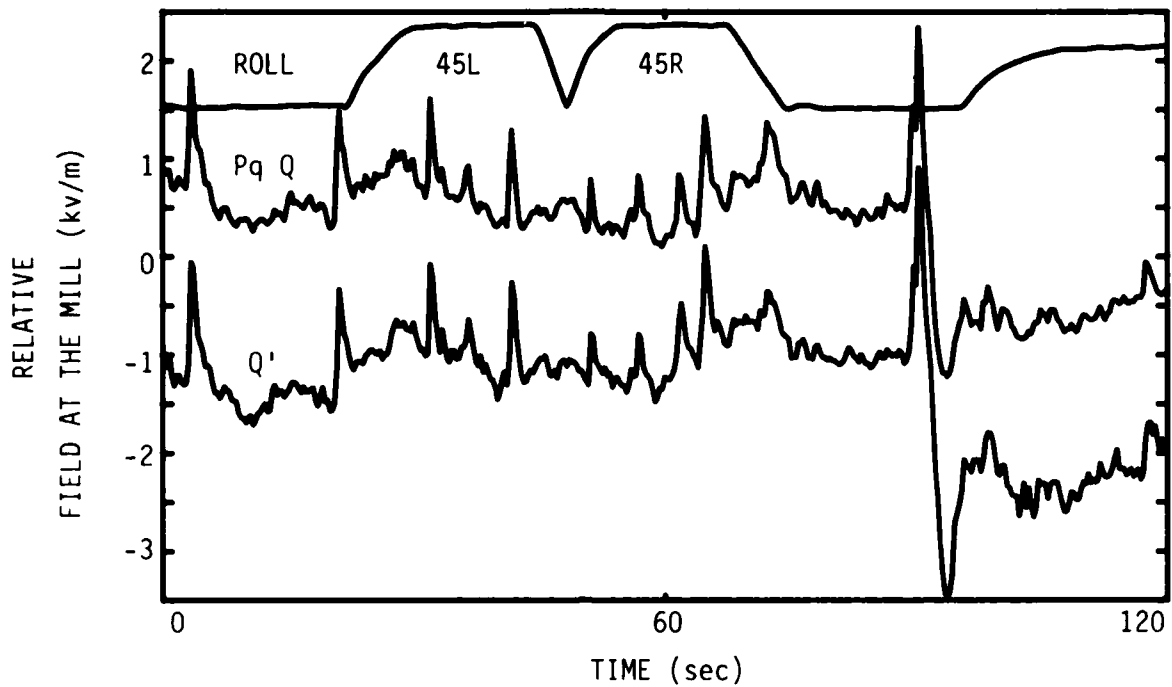
CALIBRATION FLIGHT (08/12/85)

Fig. 21 - Pz coefficient - subtracting Pq Q as measured independently from the FORWARD and TAIL mills during roll maneuvers (see text).

40

reasonable. By choosing i_c/A such that the theory and data approximately match, the results in figure 22 are obtained. I_c/A for the three cases is the same and was chosen to give the best overall fit. Obviously there is more going on than this simple model can explain; however, it does suffice to reproduce the overall shape. It should be noted that this model was not used in determining the enhancement coefficients.

Since all coefficients are now known, further refinements can be made by using the derived (from solving the matrix - eq. 8) Q to eliminate the self charge variation in all channels except Q`. An iterative approach can be taken. The values from this technique taken along with Px and Pz as discussed above are the final results for the enhancement coefficients.

The relative accuracy of an enhancement coefficient depends both on the field mill location and on the type of maneuvers performed. By far the worst coefficients are Px, Pz, and Tz. Among these the accuracy of Tz probably matters the most. This is true because its relatively larger magnitude affects the inverted matrix more. Also, from the error analysis in section VIII, it appears that changes in the error of this coefficient affect the errors in the field more than changes in the error of either Px or Pz. In general, pitch maneuvers are more difficult to perform than roll maneuvers. The pitch angle is harder to maintain (it is essential to record it), variations in altitude affect the measured external field; and, as alluded to previously, changes in the aircraft speed can change the self charge. Furthermore, a pitch maneuver cannot attain the larger angles of a roll maneuver ($\pm 15°$ versus $\pm 45°$).

Several attempts were made to obtain corroborative information of the enhancement coefficient values. Stable vertical high field conditions would give much cleaner data traces because the relative changes seen during a maneuver would be larger while the self charge variations would presumable stay the same. Near the anvil of a thunderstorm, a high field would presumably exist. There would, however, be questions as to the stability. Nevertheless, anvils were tried; however, they proved mostly unusable because conditions varied to much. Data that appeared reasonable initially turned out to be something else; for instance, the deflection observed during a roll maneuver, upon further scrutiny, failed to align with the start and the end of the roll. Presumably the aircraft was not far enough away from the turret
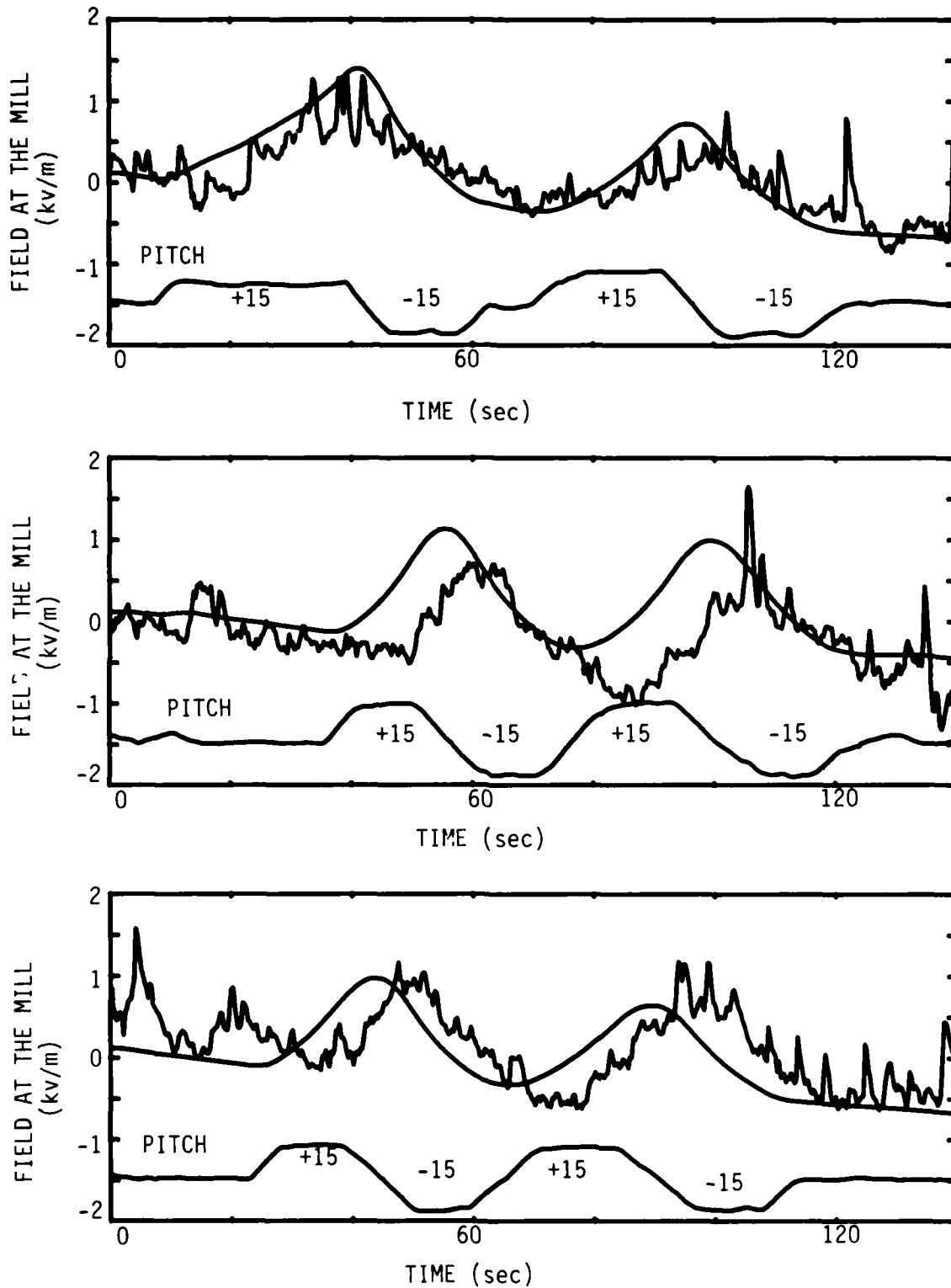
41

Fig. 22 - Modelling of self charge variations due to airspeed changes during
three different sets of pitch maneuvers. The jagged and smooth
curves are Q` and the model, respectively.

of the thunderstorm, causing a non-vertical field. What anvil results are available do, however, usually appear to give at least the right sign of a particular coefficient.

Another approach would perhaps be an examination of field changes from lightning that does not strike the aircraft. Unfortunately, because the aircraft is in corona all the time, the large field changes needed for an adequate measurement also cause changes in the self charge during the lightning discharge. The time constant for self charge is estimated from a take-off procedure (fig. 23) as less than 5 seconds. This technique might work for more sensitive ranges as we approach a storm from farther away since now the fields are less and might not affect the self charge. Corroborative information might be obtained on the Tz coefficient. The problem of the aircraft in corona was not recognized until operations had been completed. A similar technique using fast field change radiation fields has been suggested by Beasley and Master [1982]. It would require the installation of a fast field antenna at the same location as the field mill system. The magnitude of the field changes would have to be measured at a ground site. This approach might also work for slow field changes. A new design by Zaepfel [1986], which combines a field mill and slow antenna in one unit, could probably suffice for the slow field change measurement. Finally, modelling of the aircraft geometry could be examined as a comparison with the experimentally determined coefficients.

D. Values of coefficients

The final average enhancement coefficients, along with their sample standard deviations, are

$$
\begin{array}{llll}
Px= .503 \pm 1.79 & Py= 26.5 \pm 3.76 & Pz= 0 \pm 1.95 & Pv= 1.41 \pm 0.07 \\
\\
Sx= .503 \pm 1.79 & Sy= -26.5 \pm 3.76 & Sz= 0 \pm 1.95 & Sv= 1.41 \pm 0.07 \\
\\
Fx= 1.69 \pm .391 & & Fz= -4.24 \pm .854 & Fv= 0.25 \pm 0.01 \\
\\
Tx= -3.24 \pm .340 & & Tz= -3.62 \pm 1.25 & Tv= 0.32 \pm 0.02
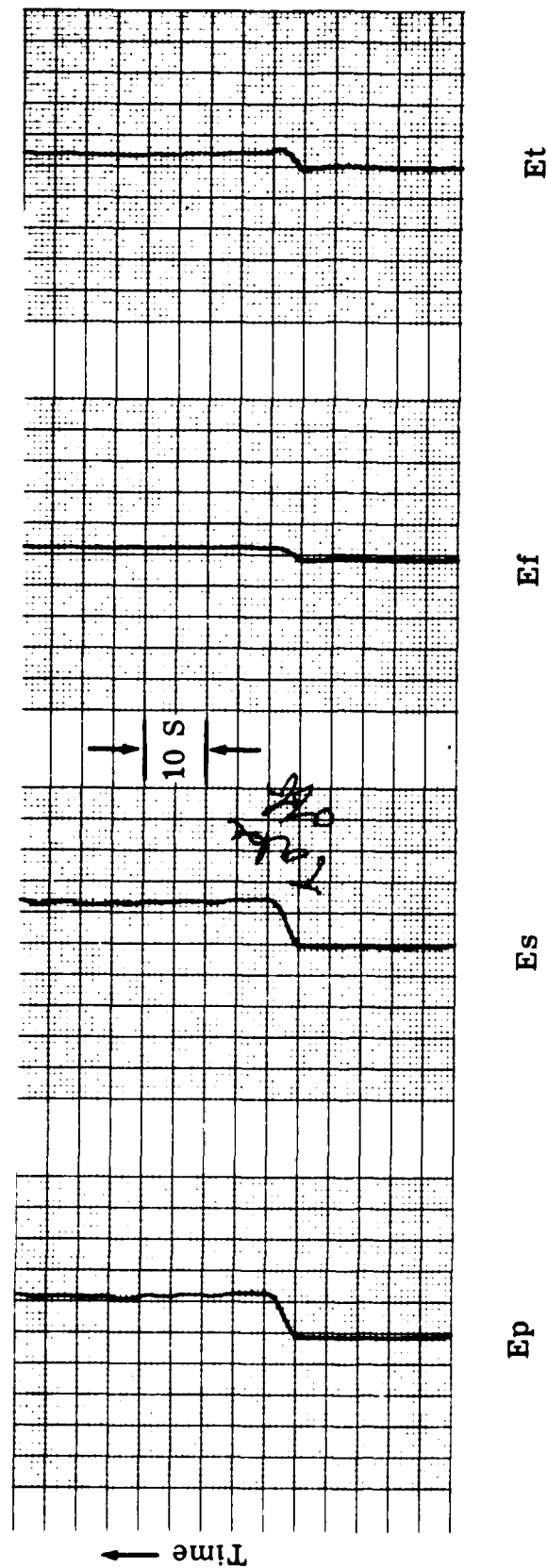\end{array}
\tag{28}
$$

Fig. 23 - Aircraft charging rate as seen in a typical data recording taken during a takeoff.

44

Since the TAIL mill is further aft of the wings, the presumed Ex nodal curve, than the FORWARD mill is ahead of them, it is reasonable to expect that Tx will be of opposite sign and larger magnitude than Fx. Similarly, since the TAIL mill is slightly closer to the Ez nodal curve than the FORWARD mill, Tz should be of same sign and slightly less in magnitude than Fz. The wingtip coefficients Px, Sx, Pz, and Sz should be close to zero because of the proximity of the wingtip meters to the wingtip nodal points. Also indicated is the stronger sensitivity of the wingtips to the self charge than the belly mills.

Since each of the coefficient values quoted in eq. 28 is actually the average of a number of independent samples, a more realistic uncertainty would be $s/\sqrt{N}$, where s is the standard deviation of the individual samples and N is the number of degrees of freedom. It is difficult to determine the appropriate value of N, however, because of the poor quality of some of the samples - especially those for Px, Pz, and Tz. Therefore, the more conservative approach of using the sample standard deviations has been chosen for the analysis below. The error estimates from this conservative approach are probably more reasonable since any reduction in uncertainties might be compensated by the neglect of other errors such as symmetry assumptions.

VIII.   ERROR ANALYSIS

Determination of the errors in the field components and the aircraft potential is not trivial because of the non-linear matrix inversion process. In eq. 2, it was assumed that the matrix elements are statistically independent. As can be seen by the explicit dependence on the enhancement coefficients in the inverted matrix (eqs. 5-8), the inverted coefficients are now statistically dependent, thus, cross terms must be considered. In order to address the problem, a Monte Carlo method has been used. First, it must be noted that due to the symmetry assumptions for the wingtip mills, Py enters only into the uncertainty associated with an Ey field. The uncertainties resulting from the method will depend on the assumed external field conditions.

The details of the analysis method entail assuming an external field and aircraft potential. The raw fields at the mill (Ep, Es, Ef, and Et) can then be calculated from the mean value of the enhancement coefficients given in eq. 28. One then constructs Gaussian generators with which the experimentally determined enhancement coefficients can be varied over their one sigma range (the standard deviation in eq. 28). There will be one such generator for each of the enhancement coefficients. A perturbed matrix, derived from these generators, is inverted to obtain a set of perturbed inverted coefficients. From this perturbed matrix and from the previously calculated fields at the mill, the perturbed external fields and aircraft potential can be calculated. The method was repeated 1000 times until the statistics were stable. The means and standard deviations for the inverted coefficients, the field components, and aircraft potential were then calculated. Several sets of input field conditions were tested so that regions of data validity could be estimated.

During each inversion, a check was made to insure that singularities did not occur (determinant of zero). Furthermore, it was determined where possible singularities could occur. This was done by holding all input coefficients except one constant and finding for what value of the free coefficient a singularity occurred. These values are given in table 1, where columns 2 and 3 are identical to the values in equation 28. The fourth column is the value for the particular coefficient which yields zero for the determinant of matrices of the form of equation 28. The last column is the absolute value of the difference between the fourth and second columns divided by the third column. This ratio indicates how far out on the wing of the distribution the singularity occurs. Assuming a normal distribution, the probability of the worst case (7.00) occurring is 2.56×10^{-12}.

The inverted coefficients and their standard deviations are

$$
\begin{array}{ccccc}
 & Ep & Es & Ef & Et \\
Ex = & (\ .008 \pm .008) & (\ .008 \pm .008) & (\ .181 \pm .060) & (-.212 \pm .038) \\
Ey = & (\ .019 \pm .003) & (-.019 \pm .003) & & \\
Ez = & (\ .024 \pm .006) & (\ .024 \pm .006) & (-.168 \pm .044) & (-.080 \pm .033) \\
V = & (\ .352 \pm .043) & (\ .352 \pm .043) & (-.065 \pm .352) & (\ .076 \pm .307)
\end{array} \tag{29}
$$

TABLE 1 - Possible singularities for inversion of enhancement coefficient matrix (See text)

ENHANCEMENT COEFFICIENT	COEFFICIENT VALUE	COEFFICIENT ERROR (1σ)	VALUE FOR DET = 0	NUMBER OF σ AWAY
Px	0.503	1.79	-62.0	34.9
Py	26.5	3.76	0	7.05
Pz	0	1.95	-20.9	10.7
Pv	1.41	0.07	-.011	20.3
Fx	1.69	.391	-3.84	14.1
Fz	-4.24	.854	1.73	7.00
Fv	0.25	0.01	15.8	1550
Tx	-3.24	0.34	1.48	13.9
Tz	-3.62	1.25	8.88	10.0
Tv	0.32	0.02	-12.9	662

Note that the errors of interest are in the fields and self charge which depend not only on the errors in the matrix elements but also on the magnitude and direction of the field and on the self charge. The direction angles are the standard azimuth-elevation coordinates as indicated in figure 24. (Note that these angles are not the same as in figure 4). The errors are listed in table 2 where some input conditions have been chosen and the relative errors calculated. The values in parenthesis are in percent for the errors of concern for a particular case. For instance, if Ex is dominant, then the relative errors in Ey and Ez do not matter. An estimate of the relative magnitude of the self charge contribution at each mill with respect to the field contributions (Vmill/Emill) has been determined as $|V|$ times the average of the absolute values of the four self charge coefficients divided by $|E|$ times the average of the absolute value of the twelve field coefficients. The result is

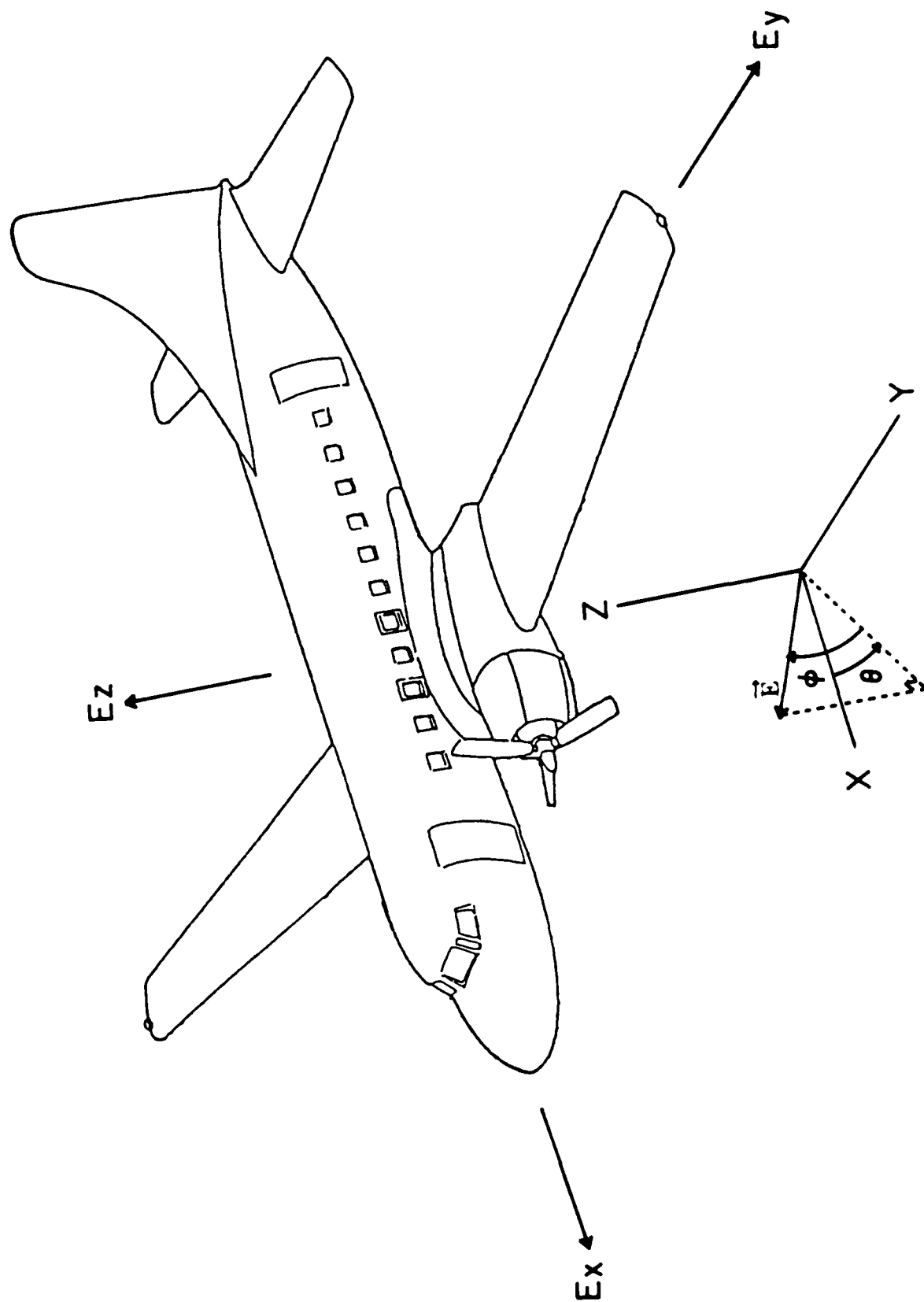$$\frac{Vmill}{Emill} = 0.152 \frac{|V|}{|E|} \tag{30}$$

Fig. 24 - Azimuth-elevation coordinate system for field magnitude and directions.

48

TABLE 2 - Errors in the external fields and aircraft self charge for some typical cases (both component and magnitude - direction are given).

RESULTING ERRORS

| CHOSEN CONDITION | | | | | | | | RESULTING ERRORS | | | | | | |
Ex	Ey	Ez	V	$\theta(^\circ)$	$\phi(^\circ)$	$\lvert E\rvert$	$\dfrac{Vmill}{Emill}$	Ex	Ey	Ez	V	$\lvert E\rvert$	$\theta(^\circ)$	$\phi(^\circ)$
1	1	1	10	45.0	35.3	1.73	.88	.371(37)	.157(16)	.269(27)	2.13(21)	.319(18)	10.9(24)	7.35(21)
10	1	1	10	5.71	5.68	10.1	.151	1.25(13)	.157	1.27	13.4	1.28(13)	1.11(19)	6.85
1	10	1	10	84.3	5.68	10.1	.151	.371	1.57(16)	.269	2.13	1.56(16)	2.23(3)	1.74
1	1	10	10	45.0	82.0	10.1	.151	3.41	.157	2.31(23)	15.5	2.57(25)	59.4	8.99(11)
1	1	1	11.4	45.0	35.3	1.73	1.00	.372(37)	.157(16)	.270(27)	2.15(19)	.320(19)	10.9(24)	7.36(21)
1	1	1	22.7	45.0	35.3	1.73	2.00	.386(39)	.157(16)	.283(28)	2.40(11)	.334(19)	11.2(25)	7.55(21)
10	10	10	10	45.0	35.3	17.3	.088	3.67(37)	1.57(16)	2.65(27)	20.4	3.13(18)	10.8(24)	7.33(21)
1	1	1	100	45.0	35.3	1.73	8.8	.626	.157	.509	5.59(6)	.554	18.6	12.1

This term does not indicate changes in errors due to different field directions. A value of one for this parameter should approximately indicate equal contributions of the aircraft potential and external fields to the meters. This case is the fifth row where the self charge is 11.4 times any of the field components. Our range of operation for (Vmill/Emill) during non-strike conditions is approximately 0 to 2. Not surprisingly, it varies dramatically during times of lightning attachment.

Errors typically are about 20% for the magnitude and direction of the external field and for the self charge. On first examination it would appear that the Ex field has the highest error (row 1); however, in comparing approximately equal field contributions in all directions versus a field in mostly one direction (rows 2 and 4), we see that the Ex field error lowers drastically (37% to 13%) while the Ez field error only lowers from 27% to 23%. This may be telling us that the worst error is really in the Ez direction. This agrees with the fact that both belly mills tend to measure the same sign of the Ez field but opposite signs of the Ex field (opposite sides of a nodal curve - thus difference techniques can be employed). It is difficult to tell at this point where a limit should be made in errors so that one component cannot be considered useful. This limit will depend to some extent on what is required from the data set - in our case we do not yet know how accurate we need to be to evaluate the triggering hypothesis. An attempt was nevertheless made to get an indication of this limit.

In figure 25, we have plotted the error budgets, in terms of percent, for Ex, Ez, θ, ϕ, $|E|$, and V, against the (Vmill/Emill) parameter for field components that are identical in all directions. The curves are plotted for constant Ex=Ey=Ez=1 while varying V. For fields in other directions, the error curves are of approximately the same shape but will be offset vertically (usually to a lower error). The error in Ey has not been included since it has a constant value of 16%. It is seen that the error on the self charge V is less than 30% for Vmill/Emill $>$ 0.5. The field error terms appear to start to increase more rapidly at about Vmill/Emill = 2.0; therefore, all components will be considered valid if 0.5 $\leq$ Vmill/Emill $\leq$ 2.0. This does not mean that the field components are not valid below 0.5 or the self charge above 2.0. Indeed, this is where these are most valid. Of particular importance are the magnitude and angle errors which are less than 25% in the above Vmill/Emill range.

50

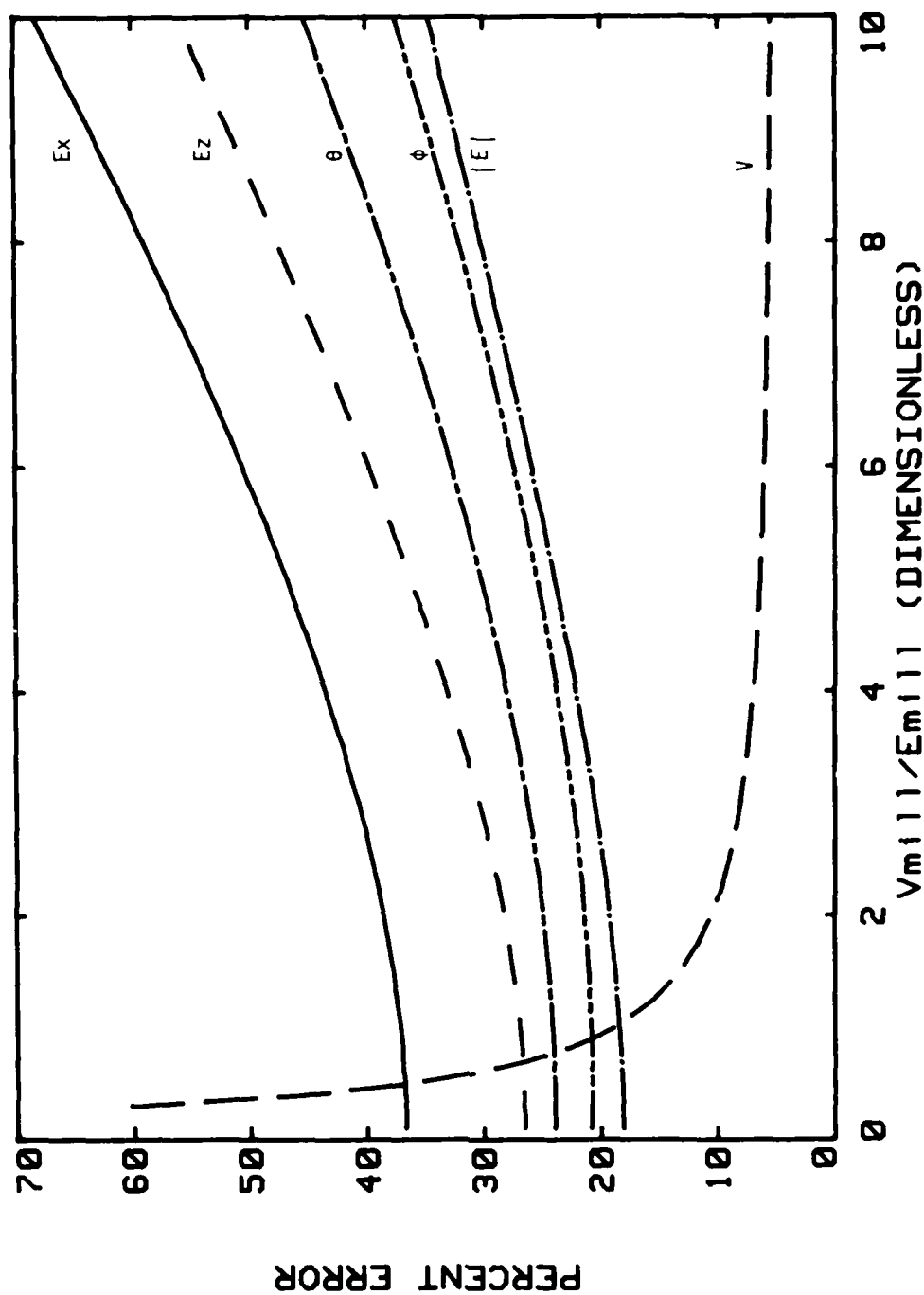ERROR PLOTS FOR DERIVED FIELDS AND SELF CHARGE
FOR A TYPICAL EXTERNAL FIELD

Fig. 25 - Error curves for an external field of Ex=Ey=Ez=1 versus the parameter Vmill/Emill (see text) while the aircraft potential V is varied.

51

IX. IMPROVEMENTS

The analysis of this data has suggested some improvements for future
reference. It appears valuable to have some redundancy in the number of
field mills to add accuracy and reliability to the results. A nose location,
although ideal for the Ex field component may have severe problems with
impaction and the need for a more powerful motor to overcome the increased
drag on the rotor caused by the aircraft movement. A better location for an
extra field meter might be on the top of the fuselage in order to provide a
meter on the opposite side of the Ez nodal curve so that the belly mills can
be differenced against it. Some provision would have to be made to prevent
this field meter from filling with water. For the CV-580, since all the
nodal points are not accessible, an optimum installation might include the
existing locations plus two extra field meters on the top of the fuselage
symmetrically above the belly meters. This would provide dual measurements
of the least accurately known fields Ex and Ez. An intriguing possibility is
to combine a nose mounted cylindrical mill with shutter mills. Finally, an
active discharger (see Pelton et. al. [1953]), if not too noisy, (or another
aircraft with a lower self charge) might aid in reducing the deleterious self
charge effects during calibrations.

X. CONCLUSIONS

The aim of this work has been the full vector calibration of an aircraft
instrumented with shutter field mills. The details involve experimentally
determining the enhancement coefficients, which when applied to the fields as
seen at the field meter locations, yield the true external field and aircraft
self charge. The two most important aspects of a successful calibration are
the initial field meter design and the choice of their locations on the air-
craft. This is probably not too surprising, but cannot be overemphasized.
Our choice of calibration procedure was an experimental calibration based on
aircraft maneuvers in the vertical fair weather field; thus our sensitivity
had to be on the order of tens of volts per meter. With a distance between
the rotor and stator of the order of mm, contact potentials can be a problem.
A contact potential of 0.1 volts gives offsets in the field of 100 V/m for a
spacing of 1 mm. A previous study [Willett + Bailey, 1983] indicates that
only stainless steel should be used in the sensing area in order to minimize

contact potentials. Field meter locations should be at 'nodal points' or at the least should be on opposite sides of nodal curves (see section IV). Unfortunately, optimum locations are not always accessible. The third major problem to overcome is the deleterious effects of self charge. This problem entails not only the reduction of the absolute level but also of the relative fluctuations in the self charge. The relatively high magnitude of the self charge seen aboard the CV-580 was reduced by attaching, in addition to the standard discharge wicks, smaller diameter (0.003 in) stainless steel wires to the aircraft. The remaining fluctuations were minimized by mixing independent measures of the self charge appropriately into the contaminated field meter outputs.

Calibration of the CV-580 aircraft has been obtained. Determination of the enhancement coefficients was not trivial since the determination required stability (or at least a measurement of the instabilities) of both the external field and the self charge during a series of maneuvers. Because the self charge fluctuations mask the fair weather signal, maneuvers are required in order to provide measurable differences in the raw outputs of the mills. The relative ratio of the enhancement coefficients was determined without knowledge of the absolute value. The absolute value was then obtained by two independent methods - direct comparison with another aircraft calibrated with respect to the vertical field and the profile technique, which involves integrating the field to the ionosphere. The absolute self charge coefficients were determined from ground measurements on insulating mats in combination with estimates of image effects from landing approaches.

After the enhancement coefficients have been found, inversion of the matrix will yield the vector field components. These inverted matrix coefficients are given in equation 29. It should be noted that the absolute value of the field components can be determined with a knowledge of only the ratios of the self charge coefficients. The external field and self charge errors are estimated from a Monte Carlo technique. The error on the magnitude of the external field is less than 25% for an aircraft potential that is not dominant ($|V|/|E| < 13.1$) and the errors in the direction angles are normally less than 10°. The error in the self charge is normally less than 20%. It is suggested that if you want to measure both the field and the self charge at the same instant with reasonable success then the condition $3.28 \leq |V|/|E|$

≤ 13.1 must be satisfied. In a companion report (Anderson + Bailey [1987], V and |E| can be found in figures 66-95. Thus |V|/|E| can easily be determined.

XI. ACKNOWLEDGMENTS

XII. REFERENCES

Ault, J. P. and S. J. Mauchly, Carnegie Institute of Washington Publication # 175, vol. 5, p. 197, 1926.

Anderson, R. V., Electrostatic Theory Applied to Helicopter Discharging, 8th International Aerospace and Ground Conference on Lightning and Static Electricity (Fort Worth), pp. 60-1 to 60-8, June 21-23, 1983.

Anderson, R. V., Measurements of Total Current Density Above Active Snowstorms, JATP, vol. 28, pp. 789 - 793, 1966.

Anderson, R. V. and J. C. Bailey, Experimental Calibration of an Aircraft Vector Electric Field Meter System, 1986 International Conference on Lightning and Static Electricity (Dayton), pp. 33-1 to 33-13, June 24 - 26, 1986a.

Anderson, R. V. and J. C. Bailey, Improved Electrostatic Discharge Wicks for Aircraft, 1986 International Conference on Lightning and Static Electricity (Dayton), pp. 49-1 to 49-5, June 24 - 26, 1986b.

Anderson, R. V. and J. C. Bailey, Vector Electric Fields Measured in a Lightning Environment, NRL Memorandum Report #5899, January, 1987.

Beasley, W. H. and M. J. Master, Merits of Supplemental Ground-Based Measurements of Lightning Electric Fields in the Interpretation of Airborne Measurements, 1982 International Conference on Lightning and Static Electricity (Oxford), March, 1982.

Bly, R. T. and J. E. Nanevicz, Aerial Measurements of the Electric Field in the Vicinity of Florida Thunderstorms: Analysis and Results, Contract NAS10-9013, SRI project 5537, Stanford Research Institute, 1977.

Boulay, J. L. and P. Laroche, Aircraft Potential Variation in Flight, 1982 International Conference on Lightning and Static Electricity (Oxford), March, 1982.

Chalmers, J. A., Atmospheric Electricity, 2nd edition, Sec. 9.19, Pergamon Press, Oxford, 1967.

Christian, H. et. al., Airborne Studies of Thunderstorm Electrification in New Mexico, Proceedings in Atmospheric Electricity, ed. by L. H. Ruhnke and J. Latham, A. Deepak Publishing, Hampton, pp. 297 - 300, 1983.

Clark, J. F., "The Fair-Weather Atmospheric Electric Potential and Its Gradient," in: Recent Advances in Atmospheric Electricity, pp. 61-73, ed. by L. G. Smith, Pergamon Press, New York, 1958.

Fitzgerald, D. F. and H. R. Byers, "Aircraft Observations of Convective Cloud Electrification," in: Recent Advances in Atmospheric Electricity, pp. 245-268, ed. by L. G. Smith, Pergamon Press, New York, 1958.

Fitzgerald, D. F. and H. R. Byers, "Aircraft Electrostatic Measurement Instrumentation and Observations of Cloud Electrification," Report Contract AF 19(604) 2189, Univ. of Chicago, 1962. (AFCRL-TR-62-805, AD-281 878)

Gunn, R., Hall, W. C., Kinzer, G. D. et. al., Technical reports on Precipitation Static, Proc. Inst. Radio Engrs., N. Y., 34, pp 156-77; 234-54, 1946.

Imianitov, I. M. and E. V. Chubarina, Electricity of the Free Atmosphere, translated from Russian, Israel Program for Scientific Translations, 1967.

Jones, J. J., C. B. Moore, Winn, W. P. and J. W. Bullock, Aircraft Measurement of the Electric Field Vector in Thunderstorms, Abstract A51B-08, EOS, vol. 66, No. 46, Page 840, Nov. 12, 1985.

Laroche, P. et. al., In Flight Thunderstorm Environmental Measurements During the Landes 84 Campaign, 10th International Aerospace and Ground Conference on Lightning and Static Electricity, Paris, pp. 59-66, 1985a.

Laroche, P., Airborne Measurements of Electrical Atmospheric Field Produced by Convective Clouds, Presented at 10th International Aerospace and Ground Conference on Lightning and Static Electricity (Paris) - (Note - To the authors' knowledge, this paper is not in print and can only be obtained directly from Laroche at ONERA), 1985b.

Markson, R., Aircraft Measurements of the Atmospheric Electrical Global Circuit During the Period 1971 - 1984, JGR, Vol. 90, No. D4, pg. 5967 - 5977, June, 1985.

Mazur, V., Ruhnke, L. H. and T. Rudolph, Effect of E-Field Mill Location on Accuracy of Electric Field Measurements With Instrumented Airplane, 1986 International Conference on Lightning and Static Electricity (Dayton), pp. 31-1 to 31-7, June 24 - 26, 1986.

Morse, P. M. and H. Feshbach, Methods of Theoretical Physics, McGraw Hill, p. 1300, New York, 1953.

Mühleisen, R. P., New Determinations of Air-Earth Current Over the Ocean and Measurements of Ionospheric Potentials, Pure Appl. Geophys., vol. 84, 112, 1971.

Pelton, F. et. al., "Investigation of Means to Maintain Zero Electrostatic Charge on Aircraft," Final Report RA-766-P-10, Cornell Aeronautical Lab. Contract AF-19(122)-475, 1953. (AD-035098)

Terman, F. E., Radio Engineers' Handbook, McGraw Hill, p. 113, New York, 1943.

Whipple, F. J. W., On the Association of the Diurnal Variation of Electric Potential Gradient in Fine Weather With the Distribution of Thunderstorms Over the Globe, Quarterly Journal of the Royal Meteorological Society, Vol. 55, p. 1-17, 1929.

Willett, J. C. and J. C. Bailey, Contact-Potential and Surface-Charge Effects in Atmospheric-Electrical Instrumentation, NRL Memorandum Report 5063, April, 1983. (AD-A 127 865)

Zaepfel, K. P., A Wide Bandwidth Electrostatic Field Sensor for Lightning Research, 1986 International Conference on Lightning and Static Electricity (Dayton), p. 32-1, June 24 - 26, 1986.

END

5-87

DTIC